WIND-INDUCED DYNAMIC RESPONSE OF BRIDGES

by

Guillaume Rousseau

Diplôme d'Ingénieur de l'Ecole Centrale des Arts et Manufactures, 2004

Submitted to the Department of Civil and Environmental Engineering
In Partial Fulfillment of the Requirements for the Degree of

Master of Engineering
In Civil and Environmental Engineering

at the

MASSACHUSETTS INSTITUTE OF TECHNOLOGY

June 2004

© 2004 Guillaume Rousseau
All Rights Reserved.

*The author hereby grants MIT permission to reproduce and distribute publicly
paper and electronic copies of this thesis document in whole or in part.*

Signature of Author_____
Department of Civil and Environmental Engineering
May 7, 2004

Certified by_____
Jerome J. Connor
Professor of Civil and Environmental Engineering
Thesis Supervisor

Accepted by_____
Heidi Nepf
Chairman, Departmental Committee on Graduate Studies

WIND-INDUCED DYNAMIC RESPONSE OF BRIDGES

by
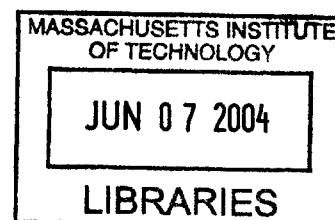
Guillaume Rousseau

Submitted to the Department of Civil and Environmental Engineering
On May 7, 2004
In Partial Fulfillment of the Requirements for the Degree of Master of Engineering
In Civil and Environmental Engineering

Abstract

Wind loading has long played a significant role in bridge design. Some spectacular failures, such as the Tay Bridge (Scotland, 1879), or the Tacoma Narrows Bridge (Washington State, 1940) acted as a painful reminder to engineers in case they had forgotten the importance of wind loading. Today, a constant drive for longer spans in suspension or cable-stayed bridges forces designers to give even more care to wind load. The Golden Gate Bridge (1280 m, San Francisco, built in 1937), which held the record for the longest span for 27 years, is now a distant 7th to the Akashi-Kaikyo (1991 m, Japan, 1998). Different in many ways, the current hunger of Japan and China for new infrastructure leads a renewal of innovation in bridge design and wind engineering. A few projects in Europe or the United States, like the Great Belt Bridge (1624 m, Denmark, 1998), or the Messina Bridge project (3300 m, Italy, not built) are part of the same trend.

The design of such a structure is a real challenge for the designer. A good example is given by the Messina Bridge in Veneziano and Van Dyck, 1998. Wind loading in different directions, determination of the reference wind speed, earthquake load, numerous cases of traffic loading ... are investigated thoroughly. The intent of this thesis is to present the essentially dynamic behavior of bridges submitted to wind. The main phenomenon involved will be exposed, as well a method to evaluate the maximum response for given wind conditions. Theories and methods developed by A.G. Davenport and R.H. Scanlan support most of the developments in this text. This thesis will not deal with specific design issues, the analysis of the response being already quite an extensive topic. Rather, its purpose is to give the reader a better understanding of wind engineering, in the belief that good design is a complete thinking process based on understanding of the underlying behavior, and not the application of straightforward recipes. This is particularly true when dealing with those high-performance structures mentioned above.

Thesis Supervisor: Jerome J. Connor
Title: Professor of Civil and Environmental Engineering

Acknowledgements

There are many people I would like to thank, for their help on this thesis, as well as for their support throughout the years, at MIT, at Centrale and at Sainte-Geneviève.

First, I would like to thank my parents. Not much would have been accomplished without your constant love and support. You always pushed me to do better, and in the meantime your care for everybody in our family was a great example to me. It would not be fair to forget my brothers and sisters, Cécile, François, Christophe, Hélène and Paul, and all the members of our family, who are the source of so many joys and a great comfort in distressing times.

Particularly, I owe a very special thanks to my four grandparents, for all their love.

I would like to thank Professor Connor, for all that I learned from him this year, for all the energy he puts in his works with students, and for his kindness and readiness to help. I would like to thank Lisa Grebner for all the help and time given to the MEng program. I would also like to thank Professor Kausel for making me discover and like Structural Dynamics, and inspiring the work of this thesis.

Finally, I want to remember the many friends I made during these years. At MIT, people from the MEng program, from Tang Hall and from TCC certainly helped make this year a great year, and friendship was never reported missing, even through the hardest times. Even away, many people from Centrale and Sainte-Genevieve remain lively in my heart. I particularly want to mention Marie Lagabrielle and Xavier Vassor, whose support and friendship are invaluable to me.

TABLE OF CONTENTS

LIST OF FIGURES

LIST OF TABLES

CHAPTER I: INTRODUCTION TO WIND AND WIND ENGINEERING

1-1 Overview

On December 28, 1879, on a stormy night, the Tay Bridge, near Dundee in Scotland collapsed, throwing into the water the train from Edinburgh and its 75 passengers. There were no survivors. The Tay Bridge, opened in February 1878, and the longest bridge in the world with its 85 spans covering 2 miles, was designed by Sir Thomas Bouch, one of the leading bridge engineers of the time. The investigation showed that bad design and construction, in conjunction with very severe weather conditions (the wind was blowing at about 25-30 m/s) caused the tragic accident. Although the exact circumstances of the accident are discusses, it is likely that the wind overturned the train, and the impact of the train on an already fragile structure, even more strained by the wind load, led to the collapse. Particularly, Bouch was blamed for designing the Tay Bridge for a wind pressure of 10 lb/sq ft instead of the 30 lb/sq ft he later used on the design of the Forth Bridge.
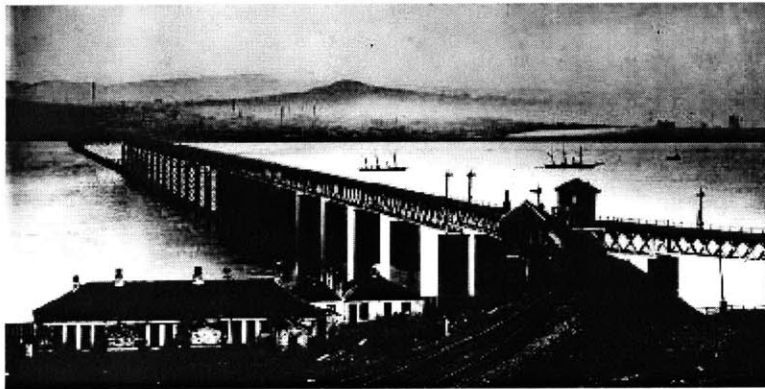
Figure 1 - 1: The Tay Bridge before the disaster

The First Tacoma Narrows Bridge (853 m) opened on July 1, 1940, and collapsed only 5 months later, on November 7, 1940, in one of the most spectacular engineering failures up to date. In fact, the bridge experienced smooth vertical vibrations during construction, which continued after opening. The amplitude of the vibrations was about

0.40 m. Before satisfactory actions were taken to mitigate the vibrations, the bridge collapsed, when submitted a wind of only 19 m/s. Indeed, on that day vertical vibrations suddenly became more violent, then combined with twisting of the deck. Ultimately, after 45 minutes of violent oscillations, the central section of the deck fell into the Puget Sound, and the rest of the deck followed quickly. Luckily there were no casualties. It turned out that engineers had completely overlooked aerodynamic effects on the bridge deck, i.e. motion-induced loads. The deck, a very simple plate girder system, had very little stiffness, both vertically and torsionally. Therefore both modes could enter resonance at low wind velocity. In addition, the narrow separation between the two modes led to a coupled resonance of the two modes, also called flutter. The influence of the Tacoma Narrows Bridge on bridge design is still very strong, as no cable-supported bridge(be it cable-stayed or suspension) presently uses a simple plate girder without stiffeners to increase torsional rigidity. The evaluation of closed box girders is a direct consequence of this collapse.

Figure 1 - 2: The collapse of the Tacoma Narrows Bridge

The last decade has seen more very long span bridges built than nearly all the century before. The Akashi-Kaikyo Bridge (1991m, Japan, 1998, suspended) now holds

the record for the longest span. The responsibility of engineers is higher than ever, in the midst of a constant drive for longer span, to ensure these bridges are safe. High amongst safety concerns, in the light of the two collapses mentioned above, is the influence of wind. Longer and lighter structures are very sensitive to wind load, and behave in ever more complex ways. It is therefore crucial for engineers to understand fully the phenomena at stake.

Figure 1 - 3: The Akashi-Kaikyo Bridge

1-2 The origin of wind

Wind is the displacement of masses of air in the atmosphere. These displacements are induced by differences in air pressure. However, wind itself modifies atmosphere pressure, creating a feedback process that explains the high complexity of weather forecasting. At high altitudes, the inertia force of Coriolis, induced by the rotation of the Earth, is the main generator and regulator of global air circulation. Extensive theories have been developed on the topic; however, these issues are beyond the scope of this text. For further information, the reader can refer for example to Lutgens, 2004. Relevant for this text is the study of wind at low altitudes (below 200m), in what is called the atmospheric boundary layer. It is very rare that bridges go beyond that height.

At the heart of wind engineering is the distinction between mean wind load and turbulent wind. Figure 1-4 underlines that distinction. Measurements of wind have been

taken. The duration of the patterns of motion that can be distinguished is plotted against their geographical scale. Two distinct phenomena appear. Mean wind is characterized by a time scale in the order of magnitude of several minutes, hours or even days, and a spatial scale of several hundred meters. For that reason, mean wind load can be described as a static load and can be considered nearly constant over the extent of the structure.
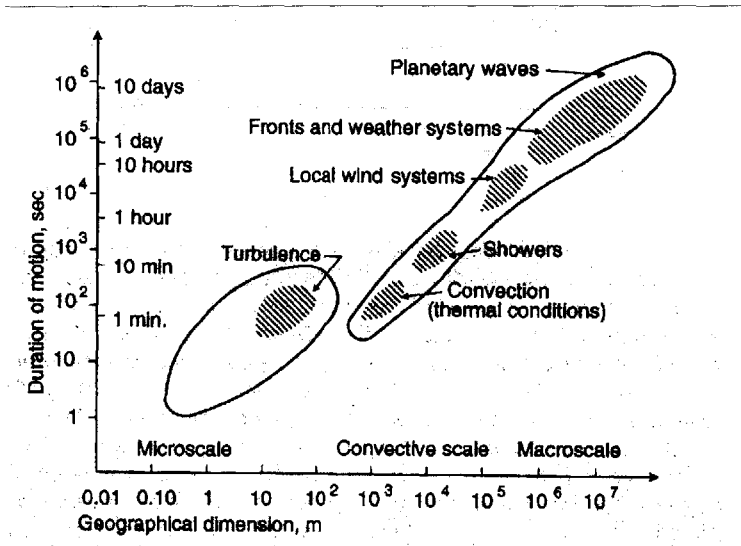
Figure 1 - 4: Order of magnitude in space and time for different patterns of motion in the atmosphere

Conversely, turbulences characteristic time is on the order of several seconds and their characteristic length is several meters long. Several conclusions can be obtained from this observation. First, there is a clear separation between the phenomenon of mean wind and turbulences. Second, response to turbulent wind load has to be studied in a dynamic way. However, it should be noticed that turbulences periods are mostly above 10s, and thus will be essentially above the natural vibration of the studied structure. This result allows for important simplifications when computing response of vibrating structures. Finally, response calculations will have to take into account the lack of correlation of wind across the structure.

1-3 Conventions

Before proceeding, it is necessary to establish some notations. First, axis of reference will be setup according to the wind direction. The x axis will be oriented in the along wind direction, the z axis in the vertical direction, and the y axis will be oriented so that the (x,y,z) frame is right-handed.
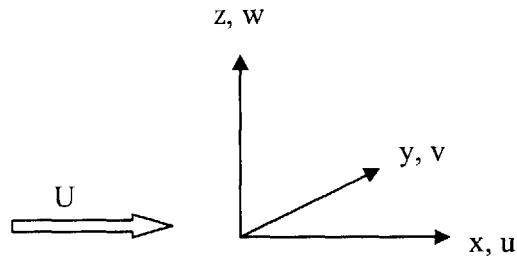
Figure 1 - 5: Spatial conventions for wind engineering

The capital letter U will characterize mean wind, while components of the turbulent wind will be named u, v and w, respectively along the x, y and z axis. U will be considered as a function of space only. u, v and w will be described as stationary stochastic processes. Stationary means that their probabilistic properties (average, standard deviation) are independent of time. This description is relatively accurate near the peak of the distribution, it can lead to significant errors for extreme values, on the tail of the distribution. The mean value of u, v and w is zero by definition. For that reason, the mean value of the total wind depends only on the mean wind and the standard deviation depends only on turbulence properties. Practically, U is determined by averaging over 10 minutes wind velocity in the wind direction. This is a standardized meteorological convention also adopted by civil engineers. Figure 1-4 shows that 10 minutes is right in the separation between mean wind and turbulent wind. u is then defined as the difference between wind velocity and mean wind velocity.

It is also necessary to define the load induced by wind. According to fluid mechanics, as described originally by Bernoulli, the wind pressure is proportional to the square of the velocity:

$$q = \frac{1}{2}\rho U_{tot}^2 \qquad (1.1)$$

where ρ is the density of air. The force due to pressure is expressed as:

$$F = \frac{1}{2}C_p A\rho U_{tot}^2 \qquad (1.2)$$

where C_p is called the shape factor and is dimensionless. C_p will be positive if the air exerts a pressure on the structure, and negative if it exerts suction. Typically, there will be pressure on the face of the structure facing the wind, and suction on the rear face. In some limited cases, C_p has been determined theoretically. For example, in the case of the thin flat plate. This example bears some interest in the perspective of bridge decks, as a reference. Moreover, over the years, a wealth of experimental measurements of shape coefficients has been accumulated. These results constitute a guidance to bridge designers when selecting a deck shape. However, ultimately, it is often necessary to conduct several wind tunnel model tests to validate the shape of the deck.

A is the area of the surface subjected to F. ρ varies with temperature and pressure. According to Cook, 1985, ρ=1.225 kg/m^3 in temperate regions and ρ=1.222 kg/m^3 in tropical hurricanes. It should also be noted that U_{tot} is the total wind velocity, including turbulent wind, and that F can be a drag force, along x, or a lift force, a cross-wind force or a moment acting on the structure. For bridge buffeting vibrations, the drag force F_D, the lift force F_L and the moment F_M about the y axis are retained. U_{tot} can be simplified, because turbulent wind components are small with respect to the mean wind:

$$U_{tot}^2 = (U+u)^2 + v^2 + w^2 \approx U^2 + 2Uu \qquad (1.3)$$

It is also useful to introduce the turbulence intensity:

$$I_u(z) = \frac{\sigma_u(z)}{U(z)} \qquad (1.4)$$

Finally, when doing modal analysis, the deflection of the structure will be given by ξ_{def}, while ξ and α will characterize the vertical and torsional mode shape.

CHAPTER II: DETERMINATION OF THE MEAN WIND SPEED

As mentioned in chapter I, this text is limited to wind in the atmospheric boundary layer. This lower part of the atmosphere, ranging from ground to 1km high, is where structures, particularly bridges, are located. Figure 1-4 shows that the horizontal characteristic length of mean wind is counted in kilometers, significantly higher than dimensions of most bridges. It is then a fairly good approximation to assume a horizontally homogeneous flow, i.e. to define the mean wind U as a function of z only. The variations of U(z) are essentially influenced by the ground surface.

2-1 Roughness length

The ground influences wind speed because it is a non-flat rough surface. Therefore the notion of roughness length, z_0, has been introduced to quantify the influence of the ground. In a simplistic way, the roughness length is the height at which the average velocity of the wind is zero, or the height of the vortices created by irregularities in the terrain. Table 2-1 shows how z_0 relates to the "shape" of the ground. In Table 2-1, α is a parameter of the power-law profile defined in Chapter 2-3. Several semi-empirical models have been developed to relate U(z) and z_0, and have been integrated in the design codes.

Table 2 - 1: Roughness lengths z_0 for different types of terrain

Roughness length z_0 (m)	Terrain type	α
0.01	Open land with little vegetation and few houses	0.12
0.05	Agricultural areas with few houses and wind breaks	0.16
0.3	Villages and agricultural areas with lots of wind breaks	0.22
1	Urban areas	0.30

The roughness length could be refined for urban areas. However, the complexity of the wind flows involved usually forces the designer to resort to wind tunnel model tests to determine the mean wind profile in urban areas.

2-2 Logarithmic profile

This first model is based on dimensional analysis:

$$U(z) = u_* \frac{1}{\kappa} \ln\left(\frac{z-d}{z_0}\right) \tag{2.1}$$

where $u_* = \sqrt{\frac{\tau_0}{\rho}}$ is the friction velocity; τ_0 is the shear stress at the ground surface; ρ is the air density; κ is von Kármán's constant, about 0.4; d is the change in base height that needs to be introduced when the total height of terrain irregularities is significantly higher than z_0. This is typically the case for wind speed above a forest, where d will be the mean height of the trees.

This model is satisfactory up to 200m, which is correct for most structures. In some cases, particularly for high-performance structures, a more complex and accurate model is required. A corrected logarithmic profile is then used:

$$U(z) = \frac{u_*}{\kappa}\left[\ln\left(\frac{z-d}{z_0}\right) + 5.75a - 1.88a^2 - 1.33a^3 + 0.25a^4\right] \tag{2.2}$$

where a is a non-dimensional factor:

$$a = \frac{z-d}{z_g} \qquad z_g = \frac{u_*}{6f_c} \tag{2.3}$$

The Coriolis parameter f_c underlines the effect of the Coriolis inertia force in the wind phenomenon. The Coriolis inertia force is created by the rotation of the earth. It balances the gradient in air pressure in geostrophic winds equilibrium. Its magnitude f_c is defined as a function of the earth rotation period Ω and the latitude λ:

$$f_c = 2\Omega \sin(\lambda) \tag{2.4}$$

14

The corrected logarithmic model was developed by Harris and Deaves in 1980. It is closer to experimental results, and is valid all along the atmospheric boundary layer. It should be noted that the last three terms are negligible below 300m.

2-3 The power-law profile

This is an empirical model that has come to use in design codes because of its very good accuracy with relation to its simplicity. It uses a reference height z_{ref}, usually 10m, and a power factor α, that depends of the roughness length z_0. See Table 2-1 for the value of α related to z_0. α is usually on the order of 1/9.

$$U(z) = (z_{ref}) \left(\frac{z}{z_{ref}} \right)^{\alpha} \qquad (2.5)$$

2-4 Comparison of the models

The three profiles detailed above have been compared in Table A-1. The profiles have been computed for roughness length z_0 of 0.01m, 0.05m and 0.3m. Latitude is 50°, friction velocity u_* is 2.0 m/s, d is 0 m, and zref is 10 m. Analysis of the results show that the three profiles are very close (less than 5% disparity) below 200m. At this altitude, it is verified that the logarithmic profile becomes too simplistic and inaccurate. The two other profiles remain close (less than 10% disparity).

It is also to be noted that for a given wind velocity at z=1 km, when leaving the atmospheric boundary layer, the higher the roughness length z_0 is, the slower the wind is near the ground.

2-5 Roughness change

Understandably, these models are defined in a "stable" environment, i.e. when only one kind of surface influences wind speed. When the wind meets a change in surface roughness, the wind profile after the change is a combination of the two profiles, before and after the change. This is also true when d is modified, i.e. when ground elevation

15

changes. An internal boundary layer appears that makes the transition between the two profiles, as described in the figure below. Such a problem is beyond the scope of this text, but the reader can refer to Plate, 1971 and Lemelin *et al.*, 1988 for additional information on the topic. Figure 2-1 explains visually the concept of internal boundary layer.
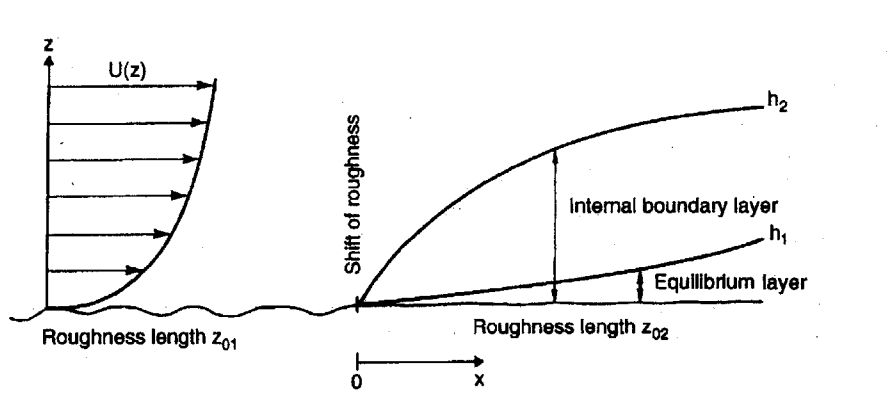
Figure 2 - 1: The internal boundary layer

2-6 Extreme wind values

These models relate in one way or another to a reference value of the wind speed, leading to an issue of scaling that is crucial for design. An accurate statistical model to predict the maximum value of the wind velocity, or more relevant, the wind pressure, is therefore a necessity.

Experience shows that wind velocity and wind pressure closely fit a Weibull distribution with shape factors respectively of 2 and 1. The Weibull distribution is defined by its density:

$$f(x) = C\frac{x^{C-1}}{A^C}\exp\left(-\left(\frac{x}{A}\right)^C\right)$$ (2.6)

where A is the shape factor and C is a scaling factor. The Weibull distribution is defined for positive values of x only.

The notion of K-years return velocity/pressure is introduced: it is the velocity/pressure that happens on average once per K years. The annual probability that this value be exceeded is 1/K. From Appendix B, Equation B.20 follows:

16

$$\frac{q(p)}{q_{50}} = \frac{1 - K_q \ln(-\ln(1-p))}{1 - K_q \ln(-\ln(0.98))} \qquad (2.7)$$

where $K_q \approx 0.2$. 50 years is the return period usually provided in wind tables as a reference. Combining this relation and reference tables, it is possible to design structures to withstand events with a specific return rate, or to evaluate the probability of failure of a structure. The designer should not forget that reference wind speeds depend not only of the location, but also of the direction of the wind. Seasonal loading is important for temporary structures.

Equation 2.7 or similar logarithmic equations are used to determine the reference pressure/velocity. If measurements are made over K years, it is possible to plot q as a function of the probability of occurrence p=n/K, where n is the number of occurrences in K years. The plot is limited to values of p above 1/K, but it is still usually possible to extrapolate and determine q_{50}. Velocity pressures are used in general for extrapolation, because it was shown (see Cook, 1985) that convergence is much faster than for wind speeds.
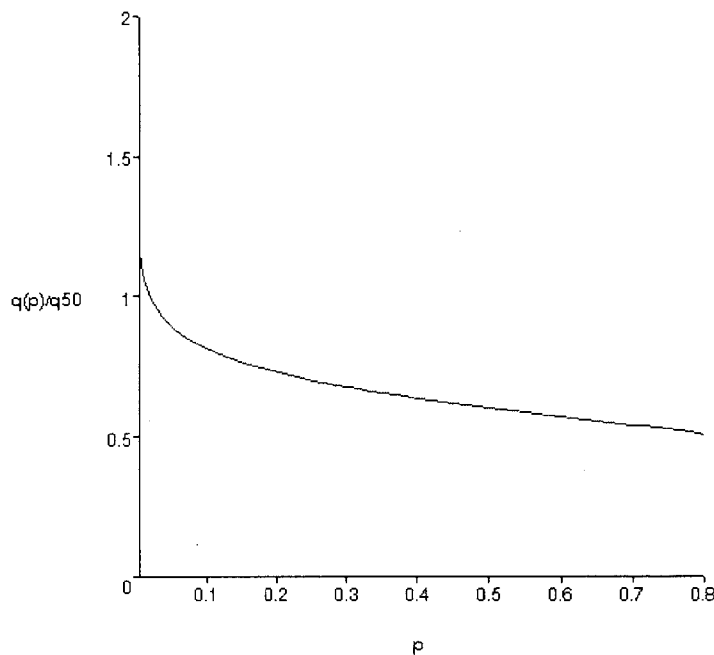
Figure 2 - 2: Velocity pressure q(p) against the probability of exceedence p

CHAPTER III: TURBULENT WIND PROPERTIES

3-1 Turbulence intensity

As seen before, turbulent wind is one of the two faces of wind. Although it is usually of less intensity, it plays a key role when considering dynamic response and eventually resonance. Turbulences are described accurately as stationary stochastic and ergodic processes. It means that characteristic properties of turbulent wind are independent of time, and can be determined by taking averages over a long enough duration.

As mentioned in Chapter 1-3, the three components of wind u, v and w have a zero mean value. Several experimental results (Davenport, 1967, Harris, 1970, Armitt, 1976) show that standard deviations decrease slowly with height, and are essentially zero above the atmospheric boundary layer, meaning there is no turbulent wind above the atmospheric boundary layer. In the lower part of the atmospheric boundary layer, where bridges lay, the standard deviations are related to the mean wind velocity (see Armitt, 1976):

$$\sigma_u = Au_* \qquad \sigma_v = 0.75\sigma_u \qquad \sigma_w = 0.5\sigma_u \qquad (3.1)$$

where A depends on the roughness length, and is equal to 2.5 for $z_0 = 0.05$m and 1.8 for $z_0 = 0.3$m. Combining these relations with the logarithmic profile, the turbulence intensity $I_u(z)$ can be related in a simple way to the altitude:

$$I_u(z) = \frac{1}{\ln(z/z_0)} \qquad (3.2)$$

for $z_0 = 0.05$m. Similar relations, with a different coefficient, can be derived for other roughness lengths.

3-2 Turbulence correlation

One way to evaluate the spatial and time correlation of turbulence is to use the integral time and length scales:

$$T(z) = \int_0^\infty \rho_u^T(z,\tau)d\tau \qquad L_u^x = \int_0^\infty \rho_u(z,r_x)dr_x \qquad (3.3)$$

where the ρ functions are the normalized autocorrelation functions:

$$\rho_u^T(z,\tau) = E\{u(x,y,z,t)u(x,y,z,t+\tau)\}\frac{1}{\sigma_u^2(z)} \qquad (3.4)$$

$$\rho_u(z,r_x) = E\{u(x,y,z,t)u(x+r_x,y,z,t)\}\frac{1}{\sigma_u^2(z)} \qquad (3.5)$$

The hypothesis of horizontally homogeneous flow and Taylor's hypothesis of "frozen turbulence" (see Batchelor, 1953) guarantee that the autocorrelation functions depend only of z and τ/r_x. It also gives the following relation:

$$L_u^x(z) = U(z)T(z) \qquad (3.6)$$

Similar quantities can be defined for v, w, or along the y and z axis.

Often, rather than determining the integral length scale from the autocorrelation function, the integral length scale is assumed, and the autocorrelation is approximated by:

$$\rho_u(z,r_x) = \exp\left(-\frac{r_x}{L_u^x(z)}\right) \qquad (3.7)$$

Again, this can be extended to other time or length scales. Counihan (1975) gives empirical expressions of the integral length scales:

$$L_u^x = Cz^m \qquad (3.8)$$

$$L_u^y \approx 0.3L_u^x \qquad L_u^z \approx 0.2L_u^x \qquad (3.9)$$

Values of C and m in Equation 3.8 are given by Figure 3.
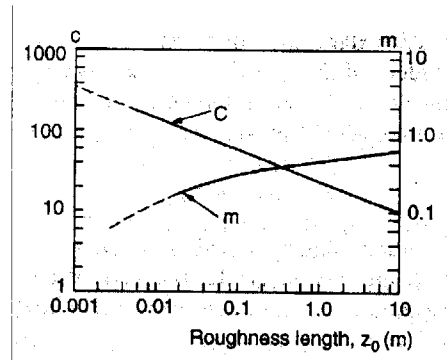
Figure 3 - 1: Values of C and m against the roughness length z_0

19

3-3 Power-spectral density function

However, the autocorrelation does not carry enough information for the purpose of wind engineering. Given that the frequency-response function H(n) is often used in the analysis, it is natural to introduce a quantity depending of frequency. The power spectrum $S_u(n)$ answers that necessity. Definitions and properties for the spectral density are provided in Appendix C. Of particular interest is Equation C.6:

$$\sigma_u^2 = \int_0^\infty S_u(n)dn \tag{3.10}$$

It is often more convenient to work with a dimensionless quantity, the power-spectral density function $R_N(z,n)$:

$$R_N(z,n) = \frac{nS_u(z,n)}{\sigma_u^2(z)} \tag{3.11}$$

The most commonly used expression for the power-spectral density function is given by Kaimal (see Kaimal *et al.*, 1972):

$$R_N(z,n) = \frac{6.8f_L}{\left(1+10.2f_L\right)^{5/3}} \tag{3.12}$$

where f_L is the non-dimensional frequency:

$$f_L = \frac{nL_u^x(z)}{U(z)} \tag{3.13}$$

3-4 Normalized co-spectrum

Another quantity appears often in wind engineering: the normalized co-spectrum of turbulence, defined in Appendix C-3. Davenport (1962) suggested a simple form of the normalized co-spectrum:

$$\psi_u(r,n) = \exp\left(-C\frac{rn}{U}\right) \tag{3.14}$$

where C is a dimensionless decay factor. Typically C=10. Extensive literature can provide more consistent but also more complex expressions of the normalized co-spectrum. See, for example, Krenk, 1995.

CHAPTER IV: DYNAMIC RESPONSE OF UNCOUPLED MODES

4-1 Probabilistic treatment of wind load

Wind load is probabilistic by nature. Therefore, it is more appropriate to deal with it in a probabilistic way than by using time-history responses that are very costly in computing power. The following method, developed by Davenport (1962) evaluates the maximum response for a given parameter R(t) as the sum of the response mean value and the standard deviation multiplied by a peak factor:

$$R_{max} = \mu_R + k_p \sigma_R \tag{4.1}$$

The peak factor k_p can be evaluated using a probabilistic model, or experimentally. It usually ranges from 3 to 5, eventually up to 10. The gust factor, characterizing both the turbulent nature of wind and the dynamic response of the structure, can then be introduced:

$$\varphi = \frac{R_{max}}{\mu_R} = 1 + k_p \frac{\sigma_R}{\mu_R} \tag{4.2}$$

The gust factor is a useful way to carry the information related to these two phenomena, letting the engineer carry then a static analysis based solely on mean wind velocity.

4-2 Determination of peak factor with a probabilistic model

Assuming that R is a Gaussian process, the normalized stochastic process Y(t) is defined by:

$$Y(t) = \frac{R(t) - \mu_R}{\sigma_R} \tag{4.3}$$

According to Cartwright and Longuet-Higgins (1956), the peak value of Y during a time T, $\mu_{Y,max}$, is asymptotically:

$$\mu_{Y,max} = \sqrt{2\ln(vT)} + \frac{\gamma}{\sqrt{2\ln(vT)}} \tag{4.4}$$

where $\gamma \approx 0.577$ is Euler's constant, and ν is called the zero-upcrossing frequency. ν is the expected number of time $X(t)$ exceeds μ_X per unit of time, and subsequently νT is the average number of zero-upcrossings during time T.

$$\nu = \sqrt{\frac{\int_0^\infty n^2 S_Y(n)dn}{\int_0^\infty S_Y(n)dn}} = \sqrt{\int_0^\infty n^2 S_Y(n)dn} \tag{4.5}$$

using Equation C.6. For a vibrating structure, ν shall be taken equal to the natural frequency n_e. Finally:

$$\mu_{X,max} = \mu_X + k_p\sigma_X = \mu_X + \mu_{Y,max}\sigma_X \tag{4.6}$$

The first equality is the definition of k_p, the second one derives directly from Equation 4.3. Then:

$$k_p = \mu_{Y,max} = \sqrt{2\ln(\nu T)} + \frac{\gamma}{\sqrt{2\ln(\nu T)}} \tag{4.7}$$

It can be observed that k_p is in the range of 3 to 5 for frequencies usual in civil engineering, i.e. from 0.1 to 10 Hz. The usual value of T is 600 s, the duration already used to determine the mean wind velocity.
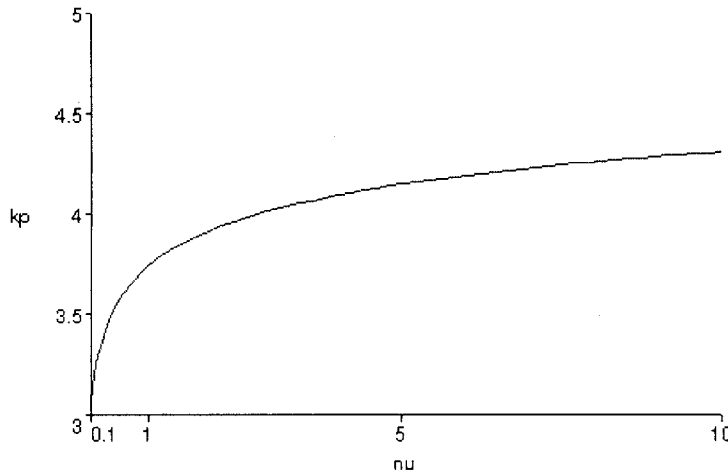
Figure 4 - 1: Peak factor k_p against zero-upcrossing frequency

To help introduce furthermore the probabilistic model developed by Davenport, two simple cases are going to be discussed before introducing the general theory.

4-3 Wind load on a static structure

The first model is a static structure submitted to wind load. Practically, this means that the structure is very stiff, i.e. its natural frequency is very high, higher than the dominant frequency of wind. Another approximation to begin is to assume the structure is point-like. A point-like structure is one where wind pressure (and velocity) can be assumed to be constant over its area A. This means that the structure characteristic length is negligible with relation to the integral length scales. Then, using relations defined in Chapter 1-3, it follows:

$$F_{tot} = F_q + F_t \tag{4.8}$$

$$F_q = \frac{1}{2} C_p A \rho U^2 \qquad F_t = C_p A \rho U u \tag{4.9}$$

The peak factor model can now be applied:

$$\mu_F = F_q \tag{4.10}$$

$$\sigma_F^2 = \int_0^\infty S_F(n)dn = \int_0^\infty \left(\frac{2F_q}{U}\right)^2 S_u(n)dn = \left(\frac{2F_q}{U}\right)^2 \sigma_u^2 \tag{4.11}$$

$$\varphi = 1 + 2k_p I_u \tag{4.12}$$

This result can now be expanded to a larger structure, but the lack of correlation between the load at different points of the structure needs to be taken into account. The maximum pressure does not apply at every point at the same time, and response computation has to acknowledge this. To simplify calculations, the structure will be considered line-like.

Using results from Appendix C-3, for I(y)=1, and Appendix D, it follows:

$$S_F(n) = \left(\frac{2F_q}{U}\right)^2 \chi^2 \left(\frac{nl}{U}\right) S_u(n) \tag{4.13}$$

where the aerodynamic admittance function χ^2 is defined by:

$$\chi^2 \left(\frac{nl}{U}\right) = \frac{2}{l} \int_0^l \left(1 - \frac{r}{l}\right) \psi_u(r,n,U)dr \tag{4.14}$$

The gust factor is then modified for large structures:

$$\varphi = 1 + 2k_p I_u \sqrt{k_b} \qquad (4.15)$$

$$k_b = \int_0^\infty \chi^2 \left(\frac{nl}{U}\right) \frac{S_u(n)}{\sigma_u^2} dn \qquad (4.16)$$

4-4 Wind load on a SDOF vibrating structure

The second example is a vibrating single degree of freedom system submitted to wind load. In this case, the relative wind speed that determines the wind load depends of the structure motion.

$$F_{tot} = \frac{1}{2} C_D A\rho \left(U + u - \dot{\xi}_{def}\right)^2 \approx \frac{1}{2} C_D A\rho \left(U^2 + 2Uu - 2U\dot{\xi}_{def}\right) \qquad (4.17)$$

The load can then be separated into mean wind load, turbulent wind load and aerodynamic damping.

$$F_q = \frac{1}{2} C_D A\rho U^2 \qquad F_t = C_D A\rho Uu \qquad c_a = C_D A\rho U \qquad (4.18)$$

The damping coefficient c_a is added to the structural damping coefficient c_s. The logarithmic decrement is then given by:

$$\delta \approx 2\pi\zeta = \frac{c_s + c_a}{2n_i m} \qquad (4.19)$$

If the drag coefficient C_D is negative, then negative damping is added to the structure. Above a certain wind speed, damping will be negative overall, causing structural instability that can lead to the collapse of the structure.

Using the approximation developed in Appendix E, results from Chapter 4-3 can be adapted:

$$\sigma_\xi^2 = |H(0)|^2 \sigma_F^2 + S_F(n_i) \int_0^\infty |H(n)|^2 dn = \sigma_F^2 + \left(\frac{2F_q}{U}\right)^2 \frac{1}{k^2} \frac{\pi^2}{2\delta_i} S_u(n_i) \qquad (4.20)$$

The gust factor for deflection is:

$$\varphi = \frac{\xi_{max}}{\mu_\xi} = 1 + k_p \frac{\sigma_\xi}{\mu_\xi} \qquad (4.21)$$

where:

$$\mu_\xi = \frac{F_q}{k} \qquad (4.22)$$

Finally:

$$\phi = 1 + 2k_p I_u \sqrt{k_b + k_r} \qquad (4.23)$$

$$k_r = \frac{n_i S_u(n_i)}{\sigma_u^2} \frac{\pi^2}{2\delta} \qquad (4.24)$$

k_b is unchanged. It is important to understand the rationale behind the approximation made in Appendix E. It distinguishes two parts in the response: the background response, where the turbulent wind is treated in a quasistatic way, and the resonant response, induced by vibrations of the structure at the resonant frequency. This approximation is valid only if the separation is clear, i.e. the frequency content of turbulent wind is below the fundamental frequency of the structure.

The results above can be extended quickly to large structures, using the aerodynamic admittance function defined in Chapter 4-3, or multiple degrees of freedom systems, using modal properties. It is important however that the modes be uncoupled, in order to be able to use the frequency response function. Response of coupled modes for bridges is treated in Chapter 5.

4-5 Gust factor for a vibrating structure

The general case is now treated: response of a parameter R(t) for a large structure. The structure is assumed to be line-like and horizontal. The influence response function is defined by:

$$R(t) = \int_0^l I_R(y) F(y, t) dy \qquad (4.25)$$

This function is defined in a static way, and normally does not take into account dynamic effects. However, the approximation in Appendix E divides the turbulent response in two parts: a quasistatic response, and a resonant response. The influence response function may be used in both cases. This is clear for the quasistatic response. For the resonant response, the reason is that mode vibration does not really deform the structure. Rather, it scales it up or down, keeping the "shape".

In the case of a line-like structure, the wind load per unit of length F(y,t) is defined by:

$$F(y,t) = \frac{1}{2}C(y)h(y)\rho\left(U(y)+u-\dot{\xi}_{def}\right)^2 \qquad (4.26)$$

where d(y) is the width of the structure perpendicular to the wind direction and C(y) is the drag coefficient. Reference values for C, d, U and I_R will be introduced in the calculations. Although it seems more complex, it leaves only dimensionless parameters in the integral. It follows:

- Mean response

$$\mu_R = \frac{1}{2}IC_{ref}d_{ref}\rho U_{ref}^2 I_{R,ref}\gamma_m \qquad (4.27)$$

$$\gamma_m = \frac{1}{l}\int_0^l g_m(y)dy \qquad g_m(y) = \frac{C(y)}{C_{ref}}\frac{d(y)}{d_{ref}}\frac{U^2(y)}{U_{ref}^2}\frac{I_R(y)}{I_{R,ref}} \qquad (4.28)$$

g_m characterizes the variation across the structure of the parameters, and γ_m gives an integral result for this variation.

- Background turbulent response

$$\sigma_b^2 = \left(IC_{ref}d_{ref}\rho U_{ref}\sigma_{u,ref}I_{R,ref}\right)^2 J_b^2 \qquad (4.29)$$

$$J_b^2 = \frac{1}{l^2}\int_0^l\int_0^l g_b(y_1)g_b(y_2)\rho_u(r_y)dy_1dy_2 \qquad g_b(y) = \frac{C(y)}{C_{ref}}\frac{d(y)}{d_{ref}}\frac{U(y)}{U_{ref}}\frac{\sigma_u(y)}{\sigma_{u,ref}}\frac{I_R(y)}{I_{R,ref}} \qquad (4.30)$$

J_b^2 can and should be computed using results of Appendix D. It is a dimensionless parameter describing variations of the response across the structure. Equation 4.30 can also be related to the method exposed in Appendix C-3. Indeed the autocorrelation is related to the normalized co-spectrum by:

$$\rho_u(r_y)\sigma_u^2(y) = \int_0^\infty S_{uu}(y_1,y_2,n)\cos(2\pi n\tau)d\tau \qquad (4.31)$$

$$S_{uu}(y_1,y_2,n) = \psi(r_y,n)\sqrt{S_u(y_1,n)S_u(y_2,n)} \qquad (4.32)$$

27

- Logarithmic decrement

The logarithmic decrement for aerodynamic damping is defined by:

$$\delta_a = \frac{\int_0^l C(y)d(y)\rho U(y)\xi(y)dy}{2n_i \int_0^l m(y)\xi^2(y)dy} \qquad (4.33)$$

It can be transformed using reduced dimensionless quantities to:

$$\delta = \delta_s + \frac{1}{2}C_{ref}\frac{U_{red}}{M_{red}}\gamma_a \qquad (4.34)$$

$$U_{red} = \frac{U_{ref}}{n_i d_{ref}} \qquad M_{ref} = \frac{m_g/l}{\rho d_{ref}^2} \qquad m_g = \int_0^l m(y)\frac{\xi^2(y)}{\xi_{ref}^2}dy$$

$$\gamma_a = \frac{1}{l}\int_0^l \frac{C(y)}{C_{ref}}\frac{d(y)}{d_{ref}}\frac{U(y)}{U_{ref}}\frac{\xi^2(y)}{\xi_{ref}^2} \qquad (4.35)$$

- Resonant turbulent response

The resonant turbulent response is caused by resonant vibrations of the structure. It can be seen as the response to the distributed load $-m(y)\ddot{\xi}_{def}(y,t)$. If the deflection is expressed as:

$$\xi_{def}(y,t) = a(t)\xi(y) \qquad (4.36)$$

then the resonant turbulent response is:

$$R_r(t) = -\ddot{a}(t)\int_0^l m(y)\xi(y)I_R(y)dy \qquad (4.37)$$

$a(t)$ is the result of the modal load $F_i(t) = \int_0^l F_t(y,t)\xi(y)dy$. In the computation of the spectral density of the acceleration, Appendix E can be used, and only the second term, the resonant one, is retained:

$$S_{\ddot{a}}(n) = (2\pi n_i)^4 \left(lC_{ref}d_{ref}\rho U_{ref}\xi_{ref}\right)^2 \left|J_y(n_i)\right|^2 S_{u,ref}(n)\frac{1}{m_i^2}\frac{n_i}{(2\pi n_i)^4}\frac{\pi^2}{2\delta} \qquad (4.38)$$

In Equation 4.38, three factors can be distinguished: $(2\pi n_i)^4$ is the factor that relates acceleration and displacement, then is the factor related to variations of the load across the structure, and finally is the integral effect of the frequency response function,

28

calculated as in Equation E.4. The logarithmic decrement is the modified decrement defined in Equation 4.34.

$$\left|J_y(n)\right|^2 = \frac{1}{I^2} \int_0^l \int_0^l g_r(y_1)g_r(y_2)\psi_u(r_y, n, U)dy_1 dy_2 \tag{4.39}$$

$$g_r(y) = \frac{C(y)}{C_{ref}} \frac{d(y)}{d_{ref}} \sqrt{\frac{S_u(y,n)}{S_u(y_{ref}, n)}} \frac{U(y)}{U_{ref}} \frac{\xi(y)}{\xi_{ref}} \tag{4.40}$$

The assumption is made that g_r is effectively independent of n, because the spectral density of u has the same dependency in n everywhere. Then:

$$\sigma_r^2 = \frac{1}{m_g^2} \left(\int_0^l m(y) \frac{\xi(y)}{\xi_{ref}} \frac{I_R(y)}{I_{R,ref}} \right)^2 \left(lC_{ref}d_{ref}\rho U_{ref}\sigma_{u,ref}I_{R,ref} \right)^2 \frac{\pi^2}{2\delta} \left|J_y(n_i)\right|^2 R_N(y_{ref}, n) \tag{4.41}$$

- Gust factor

A commonly used way of expressing the gust factor is:

$$\varphi = 1 + 2k_p I_u \sqrt{\theta_b^2 \sigma_b + \theta_b^2 \sigma_b} \tag{4.42}$$

θ_b and θ_r are introduced to describe how the variations of the parameters affect differently the mean wind response and the turbulent response. From Equations 4.27, 4.29 and 4.41, it follows:

$$k_b = \frac{J_b^2}{\gamma_b^2} \qquad \theta_b = \frac{\gamma_b}{\gamma_m} \qquad \gamma_b = \int_0^l g_b(y)dy \tag{4.43}$$

$$k_r = \frac{\pi^2}{2\delta} R_N(z_{ref}, n_i) \frac{\left|J_y(n_i)\right|^2}{\gamma_r^2} \qquad \theta_r = \frac{\gamma_r}{\gamma_m} \frac{1}{m_g} \int_0^l m(y) \frac{\xi(y)}{\xi_{ref}} \frac{I_R(y)}{I_{R,ref}} dy \qquad \gamma_r = \int_0^l g_r(y)dy \tag{4.44}$$

There are restrictions on the validity of these expressions. The γ quantities must be different from zero. This is valid if the g functions are of constant sign. If not, a case-by-case treatment is adapted. These results can be extended to plate-like structures, with the restrictions that expressions become even more complex.

CHAPTER V: AERODYNAMIC INSTABILITY OF BRIDGES

The model developed in Chapter IV is very convenient, and allows for a simple treatment of wind loading as a first approach. However, when dealing with cable-supported bridges (cable-stayed or suspension), which are very flexible structures, a number of issues arise.

In Chapter IV a simple model, dealing with forces in only one direction was introduced. In the case of bridge decks, the longitudinal component of wind induces longitudinal and vertical forces, as well as a moment. Moreover, other components of the turbulent wind need to be considered. Finally, dynamic response of a bridge deck involves significant aerodynamic feedback, which modifies the modal frequencies and damping properties of the structure, and introduces coupling between the different modes.

In the text below, h will refer to the deck height and b to its width. The wind direction is assumed perpendicular to the deck longitudinal axis. For purposes of simplicity, the horizontal deflections are assumed uncoupled from the vertical deflection and the torsion. This is not true for very long span bridges (above 1km), where horizontal deflections become significant and mode coupling in three directions can occur.

5-1 Mean wind load

As shown on Figure 5-1, the mean wind U acts in three ways on the bridge deck. U will here be defined as a function of y, because for long span bridges, the wind flow may no longer be considered horizontally homogeneous. The dependence in z is not taken into account, considering the variation in altitude of the deck, as well as the height h of the deck, are negligible. Therefore, the mean load per unit of length is defined as:

$$F_q^D(y) = \frac{1}{2}C_D h\rho U^2 \tag{5.1}$$

$$F_q^L(y) = \frac{1}{2}C_L b\rho U^2 \tag{5.2}$$

$$F_q^M(y) = \frac{1}{2}C_M b^2\rho U^2(y) \tag{5.3}$$

The shape factors C_D, C_L, C_M are functions of the angle of incidence $\alpha(y)$.
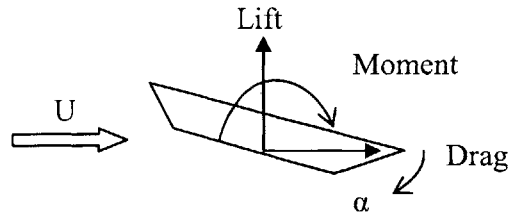
Figure 5 - 1: Forces applied on a bridge deck

5-2 Static stability of a bridge deck

Experience shows that the torsional shape factor is well approximated by a linear function of α, at least for small angles. Therefore, the governing equation for the torsional mode will be similar to:

$$I\ddot{\alpha} + k_\alpha \alpha = k_M \alpha \qquad (5.4)$$

where I is the mass-moment of inertia, k_α the structural torsional stiffness and k_M the aerodynamic torsional stiffness.

$$k_M = \frac{1}{2}\rho b^2 U^2 \frac{dC_M}{d\alpha} \qquad (5.5)$$

When k_M exceeds k_α, the solution $\alpha(t) = \exp\left[\left(k_M - k_\alpha\right)\frac{t}{I}\right]$ is a diverging exponential. Therefore, the equilibrium position α=0 is unstable, and any small perturbation could lead to the collapse of the structure. From Equation 5.5, the critical wind speed where the system becomes statically unstable is:

$$U_{div} = \sqrt{\frac{2k_\alpha}{\dfrac{dC_M}{d\alpha}\rho b^2}} \qquad (5.6)$$

5-3 Buffeting wind load

31

The buffeting wind load –buffeting is another name for turbulent wind- is more complex than the mean wind, because the angle of attack of the wind is modified by the horizontal turbulence. This modifies the shape factors, and introduces the drag coefficient in the buffeting lift load.

$$F_L(y,t) = \frac{1}{2}\rho\left[C_L(\alpha_q + \varepsilon) \times b\cos(\varepsilon) + C_D(\alpha_q + \varepsilon) \times h\right] \times \left[(U+u)^2 + w^2\right] \qquad (5.7)$$

$$F_M(y,t) = \frac{1}{2}\rho C_M(\alpha_q + \varepsilon) \times b^2 \times \left[(U+u)^2 + w^2\right] \qquad (5.8)$$

where $\alpha_q(y)$ is the angle of incidence between the mean wind and the deck, and $\varepsilon(y)$ the angle added by the turbulences. A development of the first order in ε then gives:

$$\cos(\varepsilon) \sim 1 \quad \sin(\varepsilon) \sim \frac{w}{U} \quad (U+u)^2 + w^2 \approx U^2 + 2Uu \qquad (5.9)$$

$$\begin{pmatrix} F_L \\ F_M \end{pmatrix} = \frac{1}{2}\rho U^2 b \begin{pmatrix} 2C_L & \dfrac{dC_L}{d\alpha} + C_D\dfrac{h}{b} \\ 2C_M & \dfrac{dC_M}{d\alpha}b \end{pmatrix} \begin{pmatrix} u/U \\ w/U \end{pmatrix} \qquad (5.10)$$

Values of the shape factor and their derivatives are taken for an incidence angle of α_q. The matrix coefficient relating F_X, X=L, M to the turbulence component i=u, w will be called later C_{Xi}. Of interest for a spectral density analysis is the modal load:

$$F_{i,modal}^X = \int_0^l F_X(y,t)\phi(y)dy = \frac{1}{2}\rho b \int_0^l \left[C_{Xu}u + C_{Xw}w\right]U(y)\phi(y)dy \qquad (5.11)$$

where $\Phi=\xi$, α is a mode shape. It follows, after some calculations, but very similarly to results in Chapter 5:

$$S_{XY}(n) = \left(\frac{1}{2}lb\rho U_{ref}\phi_{ref}\right)^2 \left[C_{Xu}C_{Yu}\left|J_{XY}^u\right|^2 S_{u,ref}(n) + C_{Xw}C_{Yw}\left|J_{XY}^w\right|^2 S_{w,ref}(n)\right] \qquad (5.12)$$

The cross-term of the spectral density has not been included, because it is neglected, i.e. the cross-correlation of longitudinal and vertical turbulences is negligible with relation to auto-correlations of these terms. There exist currently no quantitative results on this point. However, experience seems to confirm it indirectly. The joint acceptance functions are defined by:

$$\left|J_{XY}^i(n)\right|^2 = \frac{1}{l^2}\left|\chi_{XY}^i\right|^2 \int_0^l \int_0^l g_X^i(y_1)g_Y^i(y_2)\psi_i(r_y,n)dy_1dy_2 \qquad (5.13)$$

This function describes a double lack of correlation. There is imperfect correlation across the deck, characterized by the co-spectrum Ψ_i. But it is also necessary to take into account the fact that a bridge deck is not a line-like structure. The cross-sectional aerodynamic admittance function $\left|\chi^i_{XY}(n)\right|^2$ describes this phenomenon, i.e. the "thickness" of the deck. An analytical formulation of the aerodynamic admittance function cannot be determined because the air flows involved are too complex. It has to be determined experimentally. However, it is possible to guess its behavior. At low frequencies, the wavelength of the turbulences if great with relation to the height of the deck, and the admittance function should take values close to 1. When the frequency increases, the wavelength decreases, and so does the correlation of wind pressures. Therefore, the admittance function should take lower values. Sears, (see Sears, 1941) has provided an analytical function that seems to fit aerodynamic admittance functions for streamlined symmetric decks:

$$\chi^2_{sears}(n) = \frac{J_0(x)K_1(ix) + iJ_1(x)K_0(ix)}{K_1(ix) + K_0(ix)}$$
(5.14)

where $x = nc\pi/U$, c being the chord length of the deck. J0, J1, K0, K1 are Bessel functions of the first and second kind. Figure 5-2 shows the Sears function compared to experimental results from the Great Belt Bridge (Denmark, 1998).
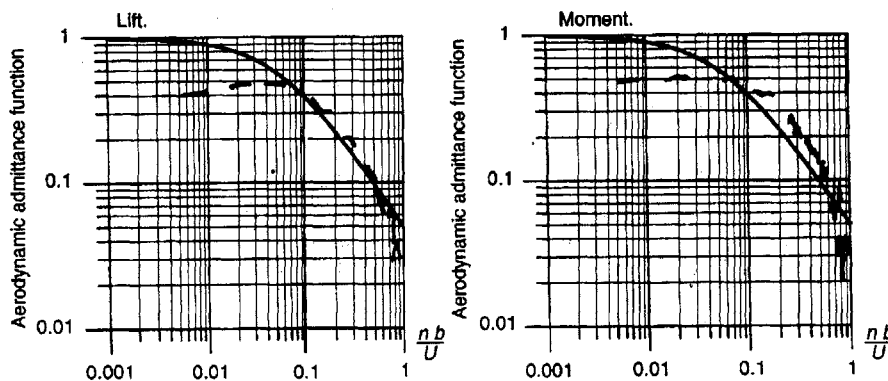
Figure 5 - 2: Aerodynamic admittance function for the Great Belt Bridge (dotted line) compared to the Sears function (solid line)

5-4 Motion-induced wind load

The motion-induced wind load is a major source of complexity and instability when dealing with bridges. The following formulation, originally developed in the field of aeronautics, was transposed to civil engineering by R.H. Scanlan (see Simiu and Scanlan, 1986). Its rationale is to linearize motion-induced wind loads with relation to the deflections.

$$F_m^L = \frac{1}{2}\rho U^2 b \left[KH_1^*(K)\frac{\dot{\xi}_{def}}{U} + KH_2^*(K)\frac{b\dot{\alpha}_{def}}{U} + K^2 H_3^*(K)\alpha_{def} + K^2 H_4^*(K)\frac{\xi_{def}}{b} \right] \quad (5.15)$$

$$F_m^M = \frac{1}{2}\rho U^2 b^2 \left[KA_1^*(K)\frac{\dot{\xi}_{def}}{U} + KA_2^*(K)\frac{b\dot{\alpha}_{def}}{U} + K^2 A_3^*(K)\alpha_{def} + K^2 A_4^*(K)\frac{\xi_{def}}{b} \right] \quad (5.16)$$

K is the reduced dimensionless frequency:

$$K = \frac{b\omega}{U} \quad (5.17)$$

The H_i^* and A_i^* are called the aerodynamic derivatives. They are functions of the geometry of the deck. They can be determined experimentally, with wind-tunnel tests. This remains the solution of choice when dealing with an innovative and performance demanding bridge. However, it is possible as a first approach to use results from previously tested design, or theoretical estimates. Particularly, results have been established for thin flat plates (see Theodorsen, 1934). These results are fairly complex, beyond the scope of this text. They provide a rough first approximation, as most decks have "better" aerodynamic properties than a thin flat plate.

Figure 5 - 3: Aerodynamics derivatives

In Figure 5-3, different results for aerodynamic derivatives have been plotted against the reduced speed $U_r = \dfrac{U}{nb}$. The solid line stands for the theoretical results for flat

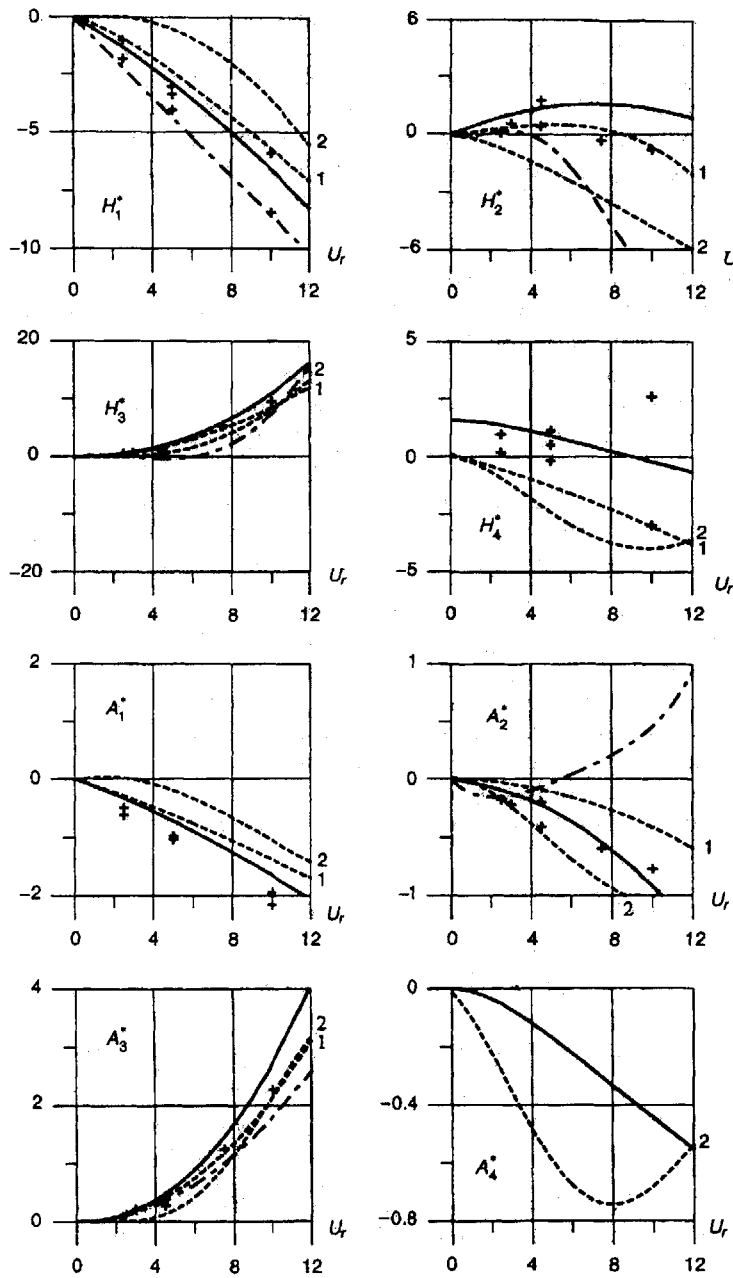plates, the long-short-long dashed line for measurements for a truss-supported girder bridge, and the other results are different sets of measurements for the Great Belt Bridge.

5-5 Modal vibrations

The loads defined above are now introduced in the behavior equations for the bridge. Because of the coupling introduced in the motion-induced wind load, the two modes considered, vertical and torsional, have to be considered together.

$$\xi_{def}(y,t) = p(t)\xi(y) \qquad \alpha_{def}(y,t) = q(t)\alpha(y) \qquad (5.18)$$

The system is then treated in the canonical way for modal analysis: multiply each equation by the corresponding mode shape, integrate in y over the extent of the bridge, and introduce the modal properties. Modal properties for the vertical and the torsional mode shape are normalized by dividing respectively by $\int_{deck} \xi^2(y)dy$ and $\int_{deck} \alpha^2(y)dy$. Normalization with respect to the deck rather than the whole bridge, simplifies modal motion-induced forces, because these affect only the deck, as it is usually by far the most flexible part of a bridge. A 2-degrees of freedom system results:

$$m_i\left(\ddot{p} + 2\zeta_\xi\omega_\xi\dot{p} + \omega_\xi^2 p\right) = F_{m,modal}^L + \frac{F_{t,modal}^L}{\int_{deck}\xi^2(y)dy} \qquad (5.19)$$

$$I_i\left(\ddot{q} + 2\zeta_\alpha\omega_\alpha\dot{q} + \omega_\alpha^2 q\right) = F_{m,modal}^M + \frac{F_{t,modal}^M}{\int_{deck}\alpha^2(y)dy} \qquad (5.20)$$

where:

$$F_{m,modal}^L = \frac{1}{2}\rho U^2 b\left[KH_1^*(K)\frac{\dot{p}}{U} + KC_\xi H_2^*(K)\frac{b\dot{q}}{U} + K^2 C_\xi H_3^*(K)q + K^2 H_4^*(K)\frac{p}{b}\right] \qquad (5.21)$$

$$F_{m,modal}^M = \frac{1}{2}\rho U^2 b^2\left[KC_\alpha A_1^*(K)\frac{\dot{p}}{U} + KA_2^*(K)\frac{b\dot{q}}{U} + K^2 A_3^*(K)q + K^2 C_\alpha A_4^*(K)\frac{p}{b}\right] \qquad (5.22)$$

The coefficients C_ξ and C_α are dimensionless. They describe the potentiality of coupling between the two modes. When $C_\xi C_\alpha$ is close to 1, the influence of cross terms in the motion-induced loads is significant, and modal vibrations are coupled. Conversely, when $C_\xi C_\alpha$ is close to 0, mode coupling is limited.

$$C_\xi = \frac{\int_{deck} \xi(y)\alpha(y)dy}{\int_{deck} \xi^2(y)dy} \qquad C_\alpha = \frac{\int_{deck} \xi(y)\alpha(y)dy}{\int_{deck} \alpha^2(y)dy} \qquad (5.23)$$

5 -6 Spectral density of buffeting vibrations, flutter wind velocity

Assuming the bridge vibrates at a circular frequency ω, Equations 5.19 and 5.20 can be transformed in a matrix equation, using the complex notation.

$$\begin{pmatrix} F_{t,modal}^L \\ F_{t,modal}^M \end{pmatrix} = A \begin{pmatrix} p \\ q \end{pmatrix} \qquad (5.24)$$

where:

$$A = \begin{pmatrix} a_{11} m_i \omega_\xi^2 \int_{deck} \xi^2(y)dy & a_{12} m_i \omega_\xi^2 \int_{deck} \xi^2(y)dy \\ a_{21} I_i \omega_\alpha^2 \int_{deck} \alpha^2(y)dy & a_{22} I_i \omega_\alpha^2 \int_{deck} \alpha^2(y)dy \end{pmatrix} \qquad (5.25)$$

$$a_{11} = -\Omega^2 + 2i\zeta_\xi\Omega + 1 - \frac{\Omega^2}{2\gamma_m}\left(H_4^* + iH_1^*\right) \qquad a_{12} = -\frac{C_\xi\Omega^2}{2\gamma_m}\left(H_3^* + iH_2^*\right)$$

$$a_{21} = -\frac{C_\alpha\Omega^2}{2\gamma_I}\left(A_4^* + iA_1^*\right) \qquad a_{22} = -\Omega^2 + 2i\zeta_\alpha\gamma_\omega\Omega + \gamma_\omega^2 - \frac{\Omega^2}{2\gamma_I}\left(A_3^* + iA_2^*\right) \qquad (5.26)$$

The following notations are introduced:

$$\Omega = \frac{\omega}{\omega_\xi} \qquad \gamma_\omega = \frac{\omega_\alpha}{\omega_\xi} \qquad \gamma_m = \frac{m_i}{\rho b^2} \qquad \gamma_I = \frac{I_i}{\rho b^4} \qquad (5.27)$$

Then the spectral density of p and q, and their cross-spectrum, are expressed as:

$$\begin{pmatrix} S_{pp} & S_{pq} \\ S_{qp} & S_{qq} \end{pmatrix} = A^{-1} \begin{pmatrix} S_{LL} & S_{LM} \\ S_{ML} & S_{MM} \end{pmatrix} \left(A^{-1}\right)^* \qquad (5.28)$$

where * is the symbol of the transconjugated matrix. The spectral densities and cross-spectrum of the buffeting loads are defined in Equation 5.12. Computation of Equations 5.12 and 5.28 allows determining numerically the critical flutter wind velocity, where vibrations of the bridge diverge. However, the procedure exposed above is computationally intensive, and its complexity hinders understanding of the physical

37

phenomena involved which is necessary to the bridge designers. The simple procedures exposed below can make it clearer.

As a final note to this procedure, wind has been assumed to come horizontally and perpendicular to the deck. However, experience as well as close inspection of the results above, particularly Equation 5.10 shows that this is the worst case scenario, and that the intensity of the load, and subsequently of the response, decrease quickly when changing the skew angle or the angle of incidence.

Equation 5.28 can be extended to more than two modes, and to take into account horizontal deflection as well, but it is at the price of added complexity. The reader can refer to Jones, Scanlan, Jain and Katsuchi, 1998, for more details.

5-7 Modifications of the dynamic properties of the deck

Modal properties of the bridge are modified by the motion-induced wind loads. Both the natural frequencies and the damping ratios are modified. For the first simple analysis that follows, mode coupling is neglected, i.e. terms in $H_2^*, H_3^*, A_1^*, A_4^*$ are not considered. Then:

$$\omega_{\xi,wind}^2 = \omega^2 - \frac{1}{2}\frac{\rho U^2}{m_i}K^2 H_4^*(K)$$ (5.29)

Equation 5.29 raises an issue when substituting for K: the in-wind frequency depends of the aerodynamic derivative H_4^* which depends itself of the in-wind frequency. Therefore, an iterative process should be used. Most often, it is not, and the following approximation is made:

$$\frac{n_{\xi,wind}^2}{n_\xi^2} H_4^*\left(\frac{U}{n_{\xi,wind}b}\right) \approx H_4^*\left(\frac{U}{n_\xi b}\right)$$ (5.30)

$$n_{\xi,wind} \approx n_\xi\sqrt{1-\frac{\rho b^2}{2m_i}H_4^*\left(\frac{U}{n_\xi b}\right)}$$ (5.31)

38

As can be seen from Figure 5-3, H_4^* is usually negative, leading to an increase in the frequency of the vertical mode. Similarly can be determined:

$$n_{\alpha,wind} \approx n_\alpha \sqrt{1 - \frac{\rho b^4}{2I_i} A_3^* \left(\frac{U}{n_\alpha b} \right)}$$ (5.32)

A_3^* is usually negative (see Figure 5-3), leading to a decrease of the torsional frequency. If the separation between the vertical and the torsional frequencies is small, it is likely that at a certain wind speed, the in-wind frequency of the two modes will coincide, creating what is called flutter vibrations. The separation ratio γ_n is a good measurement of that risk.

$$\gamma_n = \frac{n_\alpha}{n_\xi}$$ (5.33)

The risk comes when this ratio is above but close to 1. The Tacoma Narrows Bridge had a frequency ratio of 1.25, and indeed, it collapsed less than 6 months after completion, from coupled torsional and vertical oscillations. Later bridges when designed with higher ratios, close to 2, or even above, and existing bridges were rehabilitated. The usual way to achieve a higher frequency ratio is to increase torsional stiffness. Damping is also modified:

$$\zeta_{\xi,wind} = \frac{n_\xi}{n_{\xi,wind}} \zeta_\xi - \frac{\rho b^2}{4m_i} H_1^* \left(\frac{U}{n_{\xi,wind} b} \right)$$ (5.34)

$$\zeta_{\alpha,wind} = \frac{n_\alpha}{n_{\alpha,wind}} \zeta_\alpha - \frac{\rho b^4}{4I_i} A_2^* \left(\frac{U}{n_{\alpha,wind} b} \right)$$ (5.35)

In general, H_1^* is negative, which avoids risks of negative aerodynamic damping. Conversely, A_2^* is positive for non-streamlined decks, leading to a critical wind speed where aerodynamic damping outweighs structural damping:

$$A_2^* = \left(\frac{U_c}{n_{\alpha,wind}} \right) = \frac{4I_i}{\rho b^4} \zeta_\alpha \frac{n_\alpha}{n_{\alpha,wind}} = 4\gamma_i \zeta_\alpha \frac{n_\alpha}{n_{\alpha,wind}}$$ (5.36)

$$\gamma_i = \frac{I_i}{\rho b^4}$$ (5.37)

Equation 5.36 and Figure 5-3 show that an increase in the mass-moment of inertia ratio or in structural damping leads to an increase of the critical wind speed.

5-8 Coupled flutter vibrations

As mentioned in Chapter 5-6 and 5-7, flutter vibrations are coupled vibrations from the vertical and torsional mode. They are a major source of concern in the design of cable-supported bridges, because, conversely to single degree of freedom vibrations, where instability can come only from negative aerodynamic damping, the coupling of two modes is a source of instability.

A diverging state is reached when the motion-induced load adds more energy to the system than the structural damping can dissipate. Therefore, an energy method is a good way to introduce the problem. It is assumed the system is vibrating with a period T, and the lag between the vertical and the torsional mode is θ. Works are calculated over a period and for a unit length cross-section of the deck. Mode shapes are taken constant over that span. It follows:

$$\xi_{def} = \xi_0 \cos(\omega t) \qquad \alpha_{def} = \alpha_0 \cos(\omega t - \theta) \qquad (5.38)$$

$$\dot{\xi}_{def} = -\xi_0 \omega \cos(\omega t) \qquad \dot{\alpha}_{def} = -\alpha_0 \omega \sin(\omega t - \theta) \qquad (5.39)$$

$$E_{input} = \int_0^T F_m^L \dot{\xi}_{def} dt + \int_0^T F_m^M \dot{\alpha}_{def} dt = \frac{\pi}{2} \rho U^2 K^2 \xi_0 b \alpha_0 (E_{vel} + E_{def}) \qquad (5.40)$$

$$E_{vel} = (H_2^* + A_1^*)\cos(\theta) + (H_1^* \frac{\xi_0}{b\alpha_0} + A_2^* \frac{b\alpha_0}{\xi_0}) \qquad E_{def} = (-H_3^* + A_4^*)\sin(\theta) \qquad (5.41)$$

Several elements are of note in these equations. First, it should be remembered that the complex notation could not be used here, as is the rule for power calculations. Also, the deflection of a mode does not add energy to the system by itself, as is shown by the absence of term in H_4^* or A_3^*. Rather, the lag between the oscillations of the two modes modifies the level of energy in the system. Comparing Equations 5.40 and 5.41 to Figure 5-3, a parabolic shape can be derived for E_{input}.

The energy that a unit length of the system dissipates over a period through structural damping is given by:

$$E_{diss} = \int_0^T 2m_e \zeta_\xi \omega_\xi (\dot{\xi}_{def})^2 dt + \int_0^T 2I_e \zeta_\alpha \omega_\alpha (\dot{\alpha}_{def})^2 dt$$

$$E_{diss} = 2\pi \left(m_e \zeta_\xi \omega_\xi \omega \xi_0^2 + I_e \zeta_\alpha \omega_\alpha \omega \alpha_0^2 \right) \tag{5.42}$$

which is a constant with relation to U. It is then possible to solve graphically for the critical flutter wind velocity, where the two quantities are equal. The influence of θ can also be explored. θ is a function of the frequency separation γ_ω.
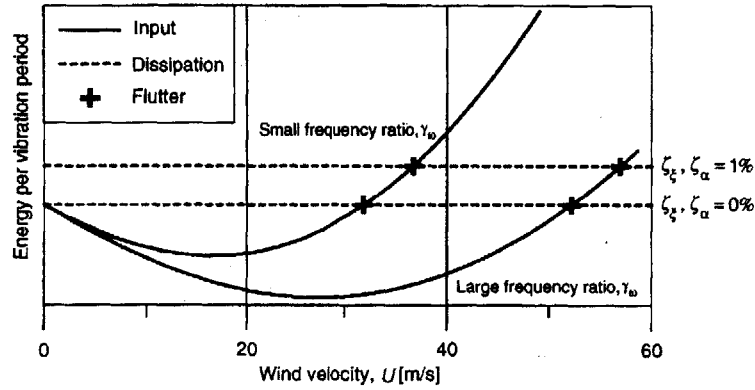
Figure 5 - 4: Graphical determination of the critical flutter wind velocity

When U exceeds the critical flutter wind velocity U_c, more energy is added to the system than it can dissipate, leading ultimately to a collapse of the structure. This is characterized by diverging solutions for the behavior equations. Using complex notation, the critical state is the one where ξ_{def} and α_{def} are of the form $Xe^{i\omega t}$, where ω is purely real. If the imaginary part of ω was positive, it would lead to a decaying solution, and if it was negative to a diverging solution. Equation 5.24 then be solved for $K_c = \dfrac{b\omega}{U_c}$. Usually, buffeting is neglected when solving for the flutter wind velocity. Therefore a solution exists when:

$$\det(A) = 0 \tag{5.43}$$

for ω real. One way to solve Equation 5.43 is to separate the real and imaginary parts, giving polynomial equations of Ω. Plotting the roots of these equations against $\dfrac{U}{nb}$ gives

two curves. Where these curves intersect is a solution of the system. This point $\left(\dfrac{U_c}{n_c b}, \Omega_c\right)$ sets the critical flutter wind velocity:

$$U_c = n_\xi b \times \frac{U_c}{n_c b} \times \Omega_c \qquad (5.44)$$

CHAPTER VI: OTHER UNSTABLE PROCESSES

Flutter is the major source of concern in bridge design. However, it would be unwise to consider it as the only issue to have in mind. There are essentially two other phenomena that should be considered: vortex shedding and galloping.

6-1 Vortex Shedding

Vortex shedding is a complex phenomenon induced by the shedding of air vortices on the sides of a structure. In general, it happens for Reynolds numbers between 30 and 5000. The Reynolds number characterizes the flow with relation to the structure:

$$Re = \frac{Ud}{v} \qquad v = \frac{\mu}{\rho} \tag{6.1}$$

where d is the width of the structure facing the wind, and v is the kinematic viscosity and μ the dynamic viscosity of air. When a vortex is created on one side of the structure, it increases the wind speed on the other side of the structure. Bernoulli's law states that:

$$p + \frac{1}{2}\rho U^2 = \text{Constant along a streamline of flow} \tag{6.2}$$

Applying Equation 6.1 to the streamline that encompasses the structure, the pressure has to decrease on the side opposite to the vortex. This creates suction on the structure, characterized by a force pulling the structure away from the vortex. As the vortices are created alternatively on one side and the other of the structure, a harmonic load is induced on the structure. The frequency of the load is equal to the frequency of the vortex shedding, thus giving the name to the phenomenon.

T. Von Kármán has studied a simple, stable form of vortex shedding, where the vortices flow away from the structure at a speed U_1, separated by a distance l_v. The alignment of vortices is called a Von Kármán vortex street. Experience shows that $U_1 \sim 0.85U$ and $l_v \sim 4.3d$, where d is the characteristic width of the structure. Therefore, the frequency n_s of the vortex shedding is given by:

$$n_s = \frac{U_1}{l_v} = St\frac{U}{d} \tag{6.3}$$

VON KARMAN VORTEX TRAIL

$30 \leq \mathcal{R}_e \leq 5000$
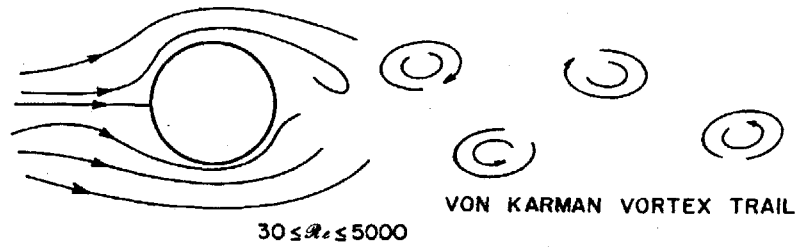
Figure 6 - 1: Von Kármán vortex street

St is the Strouhal number, and it depends on the shape of the cross-section, the turbulent wind and the surface roughness. The reader can refer to Simiu and Scanlan, 1978, for details on the Strouhal number. In the range considered, usually $St \approx 0.15$.

Three types of loads need to be considered for vortex-shedding: the lateral turbulent wind F_t (see Chapter 4), the load created by the vortex shedding F_v, and finally the aerodynamic damping created by the vortex shedding F_m.

For a bridge, the phenomenon is a bit different, in that a bridge deck is not a slender structure of width d. However, in the same way, vortices will arise in the wake of the deck, creating oscillations that can become very violent.

6-2 Load induced by vortex shedding

The load created by vortex shedding is described in a probabilistic way. Because of the complexity of the phenomenon, a purely analytical solution does not exist yet.

$$F_v(y,t) = \frac{1}{2}\rho U^2(y)d(y)C_L(y,t) \tag{6.4}$$

The lift coefficient C_L is a stochastic process, with a mean value of zero. Large-scale turbulences u'(large-scale is defined with relation to d) will affect the structure similarly to mean wind, thus modifying the frequency of the vortex shedding, and enlarging the bandwidth of frequencies covered:

$$n_s + n'_s = St\frac{U + u'}{d} \tag{6.5}$$

As turbulences are usually described by a normal distribution, the lift coefficient is also described by a normal distribution:

$$\frac{nS_{C_L}(z,n)}{\tilde{C}_L^2(z)} = \frac{n}{\sqrt{\pi}B(z)n_s(z)}\exp\left(-\left[\frac{1-n/n_s(z)}{B(z)}\right]^2\right) \tag{6.6}$$

B(z) is the spectral bandwidth. As mentioned above, the bandwidth is broadened by the intensity of turbulences, particularly large-scale. Therefore:

$$B(z) = 0.1 + 2.0I_u(z) \tag{6.7}$$

$\tilde{C}_L$ is the standard deviation of the lift coefficient. $\tilde{C}_L$ is mostly affected by small-scale turbulences. Empirical measurements show that $\tilde{C}_L$ is an increasing function of the small-scale turbulence intensity, varying between 0.10 and 0.20. For that reason, vortex shedding is particularly present when a structure is in the trail of another structure of equivalent size, because there will be more turbulences of the scale of the structure. It is to be noted that a higher standard deviation will also give higher absolute values of the lift coefficient.

6-3 Aerodynamic damping induced by vortex shedding

The complex air flows involved in vortex shedding create a significant motion-induced load F_m:

$$F_m = -h_a\ddot{\xi}_{def} - c_a\dot{\xi}_{def} \tag{6.8}$$

The added mass of air can usually be neglected, but it is not so for the aerodynamic damping. A dimensionless parameter is introduced to characterize the aerodynamic damping:

$$S_a = \frac{c_a}{\rho d^2 n_i} = \frac{2\delta_a m_i}{\rho d^2} \tag{6.9}$$

where m_i is the normalized modal mass. Similarly, the structural damping is characterized by the Scruton number:

$$Sc = \frac{2\delta_s m_i}{\rho d^2} \tag{6.10}$$

45

Typically, Sa depends of the Reynolds number and of the ratio $\dfrac{USt}{n_i d}$, which characterizes the separation between the dominant frequency of the vortex shedding and the natural frequency of the structure (See Vickery, 1978). Figure 6-2 shows that when they coincide, the negative aerodynamic damping equals the structural damping.

	Re
(Schmidt, 1965)	$0.30 - 0.75 \times 10^6$
(Szechenyi and Loiseau, 1975)	$0.8 - 3 \times 10^6$
(Szechenyi and Loiseau, 1975)	$0.8 - 3 \times 10^6$
(Yano and Takahara, 1971)	$4.0 - 9.0 z 10^4$
(Nakamura et al., 1971)	$0.7 - 4.0 \times 10^4$
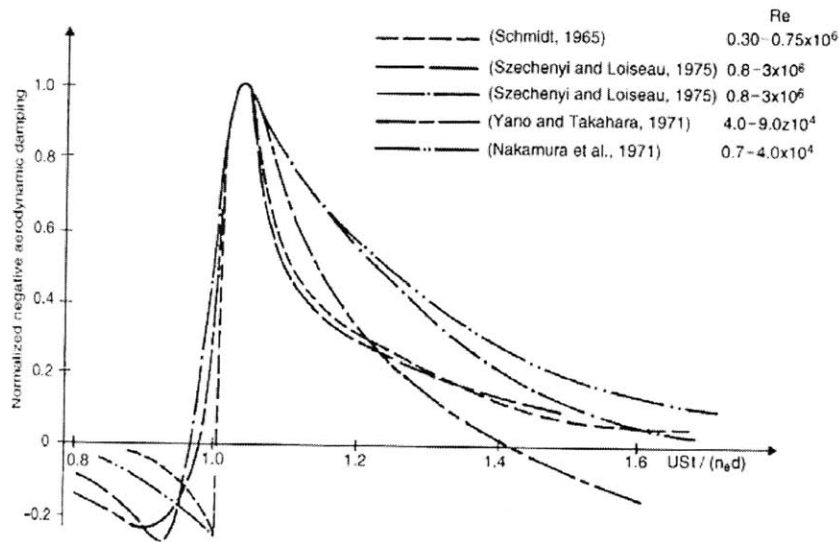
Figure 6 - 2: Normalized negative aerodynamic damping –Sa/Sc against the normalized vortex shedding frequency USt/dn$_i$

Moreover, vortex shedding is subject to the phenomenon called lock-in: in a specific frequency range, the frequency of the vortex shedding will change and "lock" on the natural frequency of the structure. Figure 6-3 clearly shows two patterns: one where the vortex shedding frequency is proportional to U/d, the Strouhal number being the proportionality factor, and one where it is equal to the natural frequency of the structure. The latter is named the "lock-in range".
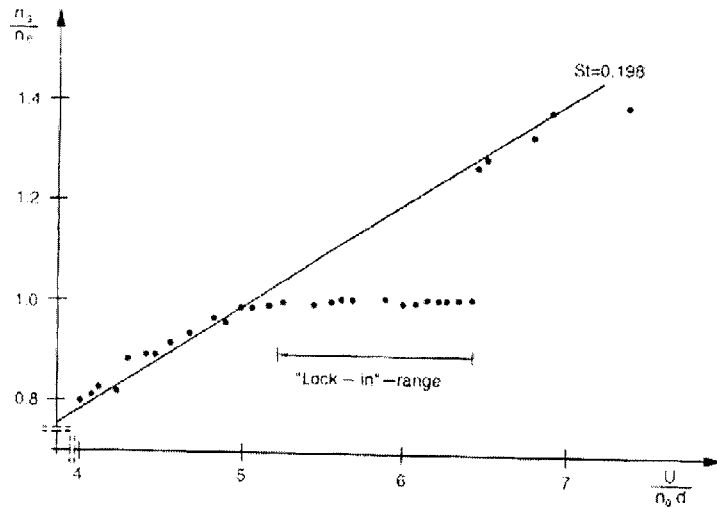
Figure 6 - 3: Normalized frequency against the reduced wind-speed

Lock-in is a complex phenomenon. Two factors are clearly identified. Smooth air flows, with reduced turbulence intensities, favor lock-in. Also, lock-in are very likely if the Scruton number for the structure is below 10, and unlikely if Sc>20. Between 10 and 20 are structures that will seem stable, eventually for a long period, until 10 or 20 years into the life of the structure, conditions will occur that will induce violent vibrations.

6-4 Galloping

Galloping is a kind of crosswind vibrations due to negative aerodynamic damping. Galloping arises when the resultant wind load is oriented in the same direction as the motion-induced wind-load.
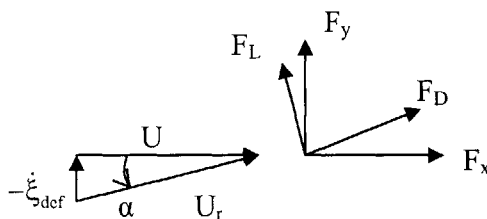
Figure 6 - 4: Force diagram for galloping

47

In the configuration described in Figure 6-4, for a structure of width d, and neglecting turbulent wind, it follows:

$$F_D = \frac{1}{2}\rho U_r^2 d C_D \qquad F_L = \frac{1}{2}\rho U_r^2 d C_L \tag{6.11}$$

where U_r is the relative wind velocity:

$$\tan\alpha = -\frac{\dot{\xi}_{def}}{U} \tag{6.12}$$

Then:

$$F_y = \frac{1}{2}\rho U^2 d C_y \qquad C_y = (C_L + C_D \tan\alpha)\frac{1}{\cos\alpha} \tag{6.13}$$

Assuming small angles, a Taylor development to the first order with relation to α can be assumed, revealing the existence of aerodynamic damping:

$$F_y = -\frac{1}{2}\rho U\dot{\xi}_{def}\left(\frac{dC_L}{d\alpha} + C_D\right)\Big|_{\alpha=0} \tag{6.14}$$

The damping coefficient will be negative if the shape factors verify the Den Hartog criterion:

$$\left(\frac{dC_L}{d\alpha} + C_D\right)\Big|_{\alpha=0} < 0 \tag{6.15}$$

In that case, the motion will diverge above a critical velocity:

$$U > U_c = -\frac{4m_i\zeta_i\omega_i}{\rho d}\frac{1}{\left(\frac{dC_L}{d\alpha} + C_D\right)\Big|_{\alpha=0}} \tag{6.16}$$

It should be noted that the shape factors depend not only of the shape of the structure, but also of the wind direction. Galloping is not as much a problem as flutter or vortex shedding. Indeed, the most common shapes cannot verify the Den Hartog criterion. However, d-shapes for example can verify it. The designer should be particularly careful with steel members, as the critical velocity is increased by increasing the mass of the structure.

CHAPTER VII: DESIGN CONSIDERATIONS

This thesis has so far been restricted to a theoretical point of view, and design issues have not been considered. It is beyond the scope of this text to present design procedures in detail, however the author would like to emphasize a few of them that are of particular importance for the designer in light of the results above.

A very detailed account of the design procedure for the Akashi-Kaikyo Bridge is given in Katsuchi, Saeki, Miyata, Sato, 1998. The Akashi-Kaikyo Bridge is an exceptional structure, and so was its design procedure (see Figure 7-1), by its complexity as well as its thoroughness. No less than 26 modes were considered in the flutter analysis, before performing large-scale wind tunnel model tests. In the case of the Akashi-Kaikyo Bridge, the model, at 1/100 scale, was 41m long and 3m wide. More and more, the emphasis will be placed on the computer analysis, keeping the wind tunnel tests to validates the process. Again, efficient use of computer analysis will come only by full understanding of the underlying phenomena, and not by simplistic application of recipes. Indeed, it is particularly striking to see how most of the limiting assumptions made in this text are not valid anymore for a structure like the Akashi-Kaikyo Bridge.

Another issue for cable-supported bridges is the lack of torsional stiffness during construction. Where truss decks present only limited resistance to wind during construction, before the structure is fully assembled and stiffened, box girders, that are widely used today, in fact because they provide more torsional stiffness than truss girders, are particularly exposed during the earliest stages of construction. During that period, the deck has only limited torsional stiffness, while it is fully resisting to wind. This makes flutter vibrations more likely. The designer should investigate carefully this issue, and eventually mitigate it. Dampers can act to limit flutter vibrations. Also, according to Tanaka, Larose and Kimura (1998), an unsymmetrical erection procedure helps preventing flutter instability.

Jones, Scanlan, Jain and Katsuchi (1998) identify at least two directions for future research in the field of bridge aerodynamics. Research on aerodynamic admittance functions and properties of turbulent wind has already been the subject of extensive efforts, and it could lead to an increase in the quality of analytical solutions.

START

Calculating Design Wind Speed

Selecting Deck Cross Section

Assuming Static Coefficient (C_D)

Calculating Design Wind Load

Analyzing Static Stress

No → Stresses Analyzed < Allowable Limit

Modification of details

Yes

Section-Model Test
(Self-excited and vortex-induced oscillation)

No → Stable or Less than Allowable Limit

Yes

Measuring Static Coefficients

Re-analyzing Static Stress and Buffeting Analysis

No → Stresses Analyzed < Allowable Stress

Yes

Checking Lateral Buckling and Divergence

No → Stable

Yes

Final Verification by Full-Model Test with Flutter & Buffeting Analyses

END

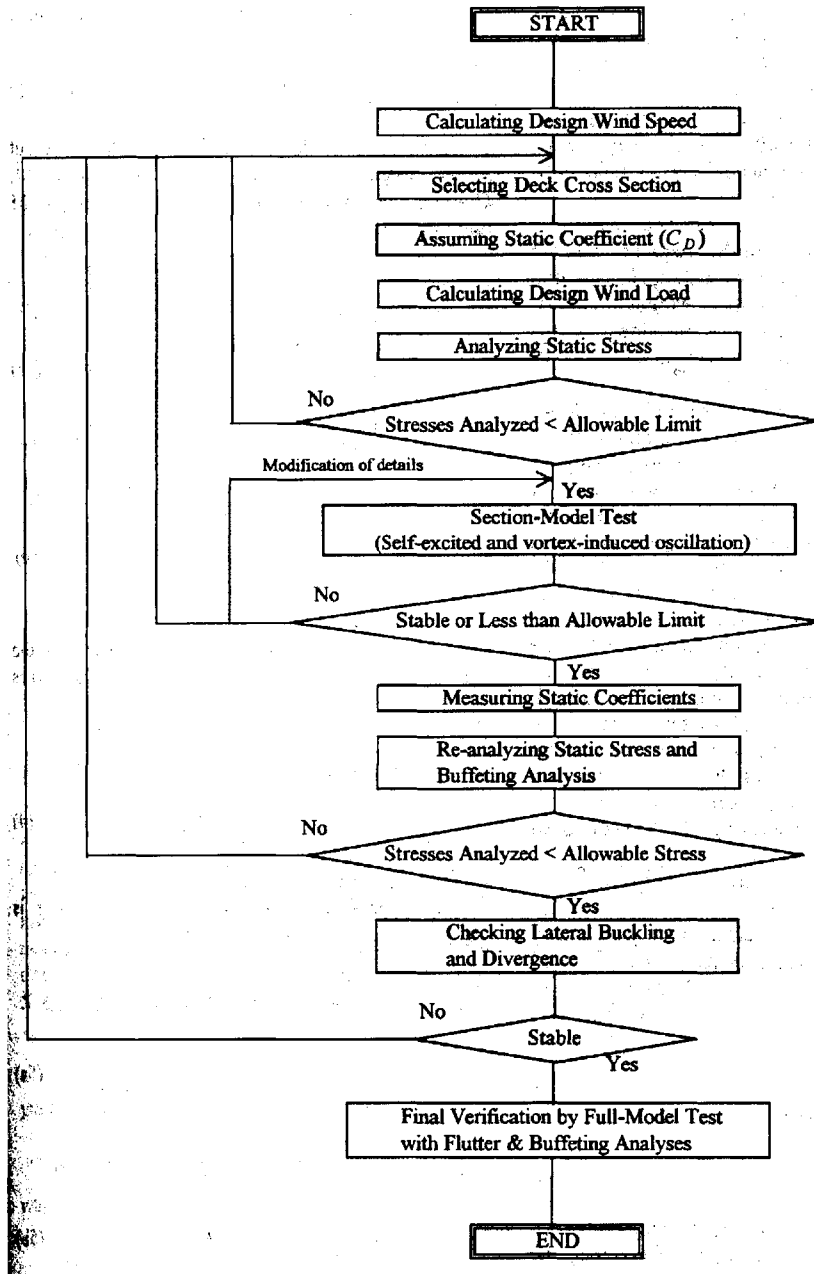Figure 7 - 1: Wind-resistant design procedure for the Akashi-Kaikyo Bridge

But they also suggest the implementation of a program to verify the wealth of existing results, analytical and from wind-tunnel tests, on one of the long span bridge recently built. This is a major challenge, by the timespan required for such a program as well as by the quantity of data that could be collected. A subsequent challenge lies in the

50

processing and analysis of that data. However, in the long term, this program could yield major results.

Finally, one of the essential parameters involved in wind-resistant design is the mean wind velocity. The design value is determined using a predictive model based on the hypothesis of stationarity: statistical properties of wind are not changing over time. However, in the current context, where global warming is likely, significant changes could occur in the weather system. This would undermine the accuracy of the predictive model. There is a major uncertainty here, and if true, it could lead to severe safety issues for the existing structures, bridges as well as buildings. Although this is contested, some studies places the first major climatic changes as soon as 2010. Considering the design-life of most bridges is now above 50 years, global warming can definitely be a threat for existing structures.

REFERENCES

Armitt, J., *Wind structures. Lecture series 89, wind effects on buildings and structures*.
Rhode-Saint-Genèse, Belgium: Von Kármán Institute for Fluid Dynamics, 1976

Batchelor, G.K., *The theory of homogeneous turbulence*.
London, England: Cambridge University Press, 1953

Cartwright, D.E., Longuet-Higgins, M.S., *The statistical distribution of the maxima of a random function*. London, England: Royal Society, 1956

Cook, N.J., *The designer's guide to wind loading of building structures, Part 1*.
Butterworths, England: Building Research Establishment, 1985

Cooper, R.G. McGillem, C.D., *Probabilistic methods of signal and system analysis (3rd edition)*. New York, NY: Oxford University Press, Inc., 1999

Counihan, J. "Adiabatic atmospheric boundary layers: a review and analysis of data from the period 1880-1972", *Atmospheric Environment* (9, p. 871-905). 1975

Davenport, A.G., "The response of slender line-like structures to a gusty wind", *Proceedings of the Institution of Civil Engineers* (23, p.389-408). 1962

Davenport, A.G., "Gust loading factors", *Journal of the Structural Division, ASCE* (93, p.11-34). 1967

Dyrbye, C., Hansen, S.O., *Wind loads on structures*.
Chichester, England: John Wiley & Sons Ltd, 1997

Harris, R.I., "The nature of the wind", *Seminar on Modern Design of Wind-Sensitive Structures, 1970* (p.29-55). London: Construction Industry Research and Information Association, 1970

Harris, R.I., Deaves, D.M., "The structure of strong winds", *Wind Engineering in the Eighties: Proceedings of the CIRIA Conference held on 12-13 November 1980*. London, England: Construction Industry Research and Information Association Paper 4, 1980

Helsinki University of Technology, *World's longest bridge spans* (cited 2004, May 7th, updated 2003, November 7th). <http://www.hsba.go.jp/bridge/e-akasi.htm>

Honshu-Shikoku Bridge Authority, *Akashi Kaikyo bridge* (cited 2004, May 7th).
<http://www.hsba.go.jp/bridge/e-akasi.htm>

Howie, J.M., *Complex analysis*.
New York, NY: Springer, 2003

Jones, N.P., Scanlan, R.H., Jain, A., Katsuchi, H., "Advances (and challenges) in the prediction of long-span bridges response to wind". In Larsen A., Esdahl S. (Eds.), *Bridge aerodynamics* (p.59-85). Brookfield, VT: A.A. Balkema, 1998

Kaimal, J.C., Wyngaard, J.C., Izumi, Y., Coté, O.R., "Spectral characteristics of surface-layer turbulence", *Journal of the Royal Meteorological Society* (98, p.563-589). 1972

Kappos, A.J., *Dynamic loading and design of structures*.
New York, NY: Spon Press, 2002

Katsuchi, H., Saeki, S., Miyata, T., Sato, H., "Analytical assessment in wind-resistant design of long span bridges in Japan". In Larsen A., Esdahl S. (Eds.), *Bridge aerodynamics* (p.87-98). Brookfield, VT: A.A. Balkema, 1998

Kausel, E., Roësset, J.M., *Advanced Structural Dynamics*.
Unpublished, Massachusetts Institute of Technology, 2001

Krenk, S., "Wind field coherence and dynamic wind forces". In Naess, Krenk (Eds.), *Symposium on the Advances in Nonlinear Stochastic Mechanics*. Dordrecht, Netherlands: Kluwer, 1995

Lemelin, D.R., Surry, D., Davenport, A.G., "Simple approximations for wind speed-up over hills", *Journal of Wind Engineering and Industrial Aerodynamics* (28, p.117-127). 1988

Lutgens, F.K., Tarbuck, E.J., *The atmosphere: an introduction to meteorology*.
Upper Saddle River, NJ: Prentice Hall, 2004

Martin, T., *Tom Martin's Tay bridge disaster web page* (cited 2004, May 7th).
<http://www.tts1.demon.co.uk/tay.html>

O'Connor, C., Shaw, P.A., *Bridge loads*.
New York, NY: Spon Press, 2000

Plate, E.J., *Aerodynamic characteristics of atmospheric boundary layers*.
Washington, DC: Atomic Energy Commission, 1971

Sears, W.R., "Some aspects of non-stationery airfoil theory and its practical applications", *Journal of Aeronautical Science* (8, p.104-108). 1941

Simiu, E., Scanlan, R.H., *Wind effects on structures : an introduction to wind engineering*.
New York, NY: John Wiley & Sons Inc., 1978

Simiu, E., Scanlan, R.H., *Wind effects on structures : an introduction to wind engineering*.
Second Edition. New York, NY: John Wiley & Sons Inc., 1986

Tanaka, H., Larose, G.L., Kimura, K., "Aerodynamics of long-span bridges during erection". In Larsen A., Esdahl S. (Eds.), *Bridge aerodynamics* (p.119-127). Brookfield, VT: A.A. Balkema, 1998

Theodorsen, T., "General theory of aerodynamic instability and the mechanism of flutter", *NACA Report No. 496*. Washington, DC: 1934

University of Washington Libraries, *History of the Tacoma Narrows Bridge* (cited 2004, May 7th, updated 2002, October 25th). <http://www.lib.washington.edu/specialcoll/tnb/>

Veneziano, D.,Van Dyck, J., "Risk analyses for the Messina bridge". In Larsen A., Esdahl S. (Eds.), *Bridge aerodynamics* (p.23-48). Brookfield, VT: A.A. Balkema, 1998

Vickery, B.J., "A model for the prediction of the response of chimneys to vortex shedding", *Proceedings of the 3rd International Chimney Design Symposium, Munich.* 1978

Waterloo Maple Inc., *Maple.* Computer Software. Waterloo Maple Inc., 2004

Appendix A

Table A-1: Comparison of values of $U/U(z_{ref})$ for the logarithmic profile, the corrected logarithmic profile and the power-law profile

z_0 (m)	0.01			0.05			0.3		
z (m)	L	CL	PL	L	CL	PL	L	CL	PL
5	0.90	0.90	0.92	0.87	0.87	0.90	0.80	0.80	0.86
10	1.00	1.00	1.00	1.00	1.00	1.00	1.00	1.00	1.00
20	1.10	1.10	1.09	1.13	1.13	1.12	1.20	1.20	1.16
30	1.16	1.16	1.14	1.21	1.21	1.19	1.31	1.32	1.27
40	1.20	1.21	1.18	1.26	1.27	1.25	1.40	1.41	1.36
50	1.23	1.24	1.21	1.30	1.32	1.29	1.46	1.48	1.42
100	1.33	1.36	1.32	1.43	1.47	1.45	1.66	1.70	1.66
150	1.39	1.43	1.38	1.51	1.56	1.54	1.77	1.84	1.81
200	1.43	1.48	1.43	1.57	1.63	1.61	1.85	1.95	1.93
250	1.47	1.53	1.47	1.61	1.69	1.67	1.92	2.04	2.03
300	1.49	1.57	1.50	1.64	1.74	1.72	1.97	2.12	2.11
500	1.57	1.69	1.60	1.74	1.90	1.87	2.12	2.36	2.36
1000	1.67	1.90	1.74	1.87	2.18	2.09	2.31	2.77	2.75
$U_L(10)$	34.54			26.49			17.53		
$U_{CL}(10)$	34.63			26.59			17.63		
α	0.12			0.16			0.22		

κ	0.4
Ω (rad/s)	7.27E-05
λ (°)	50
f_c (s^{-1})	1.11E-04
u_* (m/s)	2
z_g (m)	2.99E+03
d (m)	0
z_{ref} (m)	10

L	Logarithmic profile
CL	Corrected logarithmic profile
P	Power-law profile

APPENDIX B: DETERMINATION OF EXTREME VALUES FOR WIND VELOCITY AND PRESSURE

B-1 The Weibull distribution

The wind velocity and the wind pressure are found experimentally to fit closely a Weibull distribution, with shape factors respectively of 2 and 1. The Weibull distribution is defined, only for positive values of x, by its probability density:

$$f_X(x) = C \frac{x^{C-1}}{A^C} \exp\left(-\left(\frac{x}{A}\right)^C\right) \qquad (B.1)$$

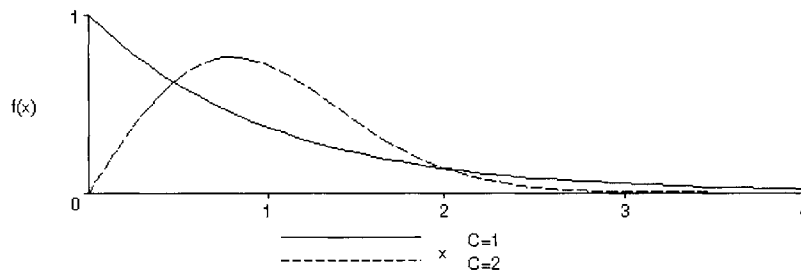A is the shape factor mentioned above, and C is a scale factor.

Figure B - 1: Probability density functions of Weibull distributions

Using the gamma function defined for positive values of x by:

$$\Gamma(x) = \int_0^\infty t^{x-1} e^{-t} dt \qquad (B.2)$$

the mean value and the variance are given by:

$$\mu_X = A\Gamma\left(1 + \frac{1}{C}\right) \qquad \sigma_X^2 = A^2\left(\Gamma\left(1 + \frac{2}{C}\right) - \Gamma^2\left(1 + \frac{1}{C}\right)\right) \qquad \text{(B.3)}$$

Extensive literature exists about the gamma function. The reader could refer for example to Howie, 2003 In the present case, only the following relations are necessary:

$$\Gamma(x+1) = x\Gamma(x) \qquad \Gamma\left(\frac{1}{2}\right) = \sqrt{\pi} \qquad \text{(B.4)}$$

Applied for q and U, it follows:

	C	μ_X/A	σ_X^2/A^2
U	2	$\sqrt{\pi}/2$	$1 - \pi/4$
q	1	1	1

Table B - 1: Mean and standard deviation of wind velocity and pressure

B-2 Derivatives of a stochastic process

In this part is considered a stochastic process X(t) (q or U for example) that can be differentiated with respect to t. The autocorrelation function $\kappa(\tau)$ is also assumed differentiable with respect to τ. It is then possible to define:

$$\dot{X}(t) = \frac{dX(t)}{dt} \qquad \text{(B.5)}$$

Considering $X(t_2) - X(t_1) = \int_{t_1}^{t_2} \dot{X}(t)dt$, the mean value of $\dot{X}$ $\mu_{\dot{X}}$ is zero. Then:

$$\frac{d\kappa(\tau)}{d\tau} = E\left\{(X(t) - \mu_X)\dot{X}(t+\tau)\right\} = \kappa_{X\dot{X}}(\tau) \qquad \text{(B.6)}$$

$\kappa(\tau) = \kappa(-\tau)$ therefore κ is an even function of τ, and its derivative in 0 is 0. Then:

$$\kappa_{X\dot{X}}(0) = 0 \qquad \text{(B.7)}$$

A stochastic process and its derivative have no statistical correlation when measured at the same time. This result is essential in the theory of extreme values, which involves derivatives of stochastic processes.

57

B-3 Expected number of crossings of a high threshold per unit of time

Considering an short span of time Δt, and a threshold ξ, the expected number of upcrossings v_ξ of ξ per unit of time is given by:

$$v_\xi dt = P\left\{X(t) < \xi \text{ and } X(t + \Delta t) \geq \xi\right\} \qquad (B.8)$$

Then:

$$v_\xi = \lim_{dt \to 0} \frac{1}{\Delta t} P\left\{X(t) < \xi \text{ and } X(t + \Delta t) \geq \xi\right\} \qquad (B.9)$$

Linearizing $X(t+dt)$ as $X(t) + \Delta t \dot{X}(t)$ and introducing the probability density function of X, it follows:

$$v_\xi = \lim_{dt \to 0} \frac{1}{\Delta t} \int_0^\infty \int_{\xi - \Delta t \dot{X}(t)}^\xi f_{X\dot{X}}(x, \dot{x}) dx d\dot{x} \approx \int_0^\infty \dot{X}(t) f_{X\dot{X}}(\xi, \dot{x}) d\dot{x} \qquad (B.10)$$

From Equation B.7, it is known that X and $\dot{X}$ are statistically independent. Therefore v_ξ is given by:

$$v_\xi = f_X(\xi) \int_0^\infty u f_{\dot{X}}(u) du \qquad (B.11)$$

For the velocity pressure, that fits a Weibull distribution with a shape factor of 1, $f_X(\xi) = \frac{1}{\sigma_X} \exp\left(-\frac{\xi}{\sigma_X}\right)$. Assuming $\dot{X}$ fits a Gaussian distribution, it follows:

$$v_\xi = \frac{1}{\sqrt{2\pi}} \frac{\sigma_{\dot{X}}}{\sigma_X} \exp\left(-\frac{\xi}{\sigma_X}\right) \qquad (B.12)$$

B-4 K-years threshold

Now the hypothesis of high thresholds leads to the following assumptions:

- The upcrossings are mutually independent.
- The probability of an upcrossing between t and t+dt is proportional to dt and independent of t.
- The probability of more than 1 upcrossing during dt is negligible.

Then $P(1,dt)=v_\xi dt$ and $P(0,dt)$. This is characteristic of a Poisson process. Then:

$$P(r,t) = \frac{(v_\xi t)^r}{r!} \exp(-v_\xi t) \tag{B.13}$$

Particularly, the probability that a threshold be exceeded during a period of duration t is given by:

$$F(t) = 1 - P(0,t) = 1 - \exp(-v_\xi t) \tag{B.14}$$

It is then possible to derive the corresponding probability density function f(t) and the average time μ_t before an upcrossing:

$$f(t) = v_\xi \exp(-v_\xi t) \tag{B.15}$$

$$\mu_t = \int_0^\infty t f(t) dt = \frac{1}{v_\xi} \tag{B.16}$$

The threshold that gives an average of K years is called the K-years threshold ξ_K. It can be a velocity or a pressure. For velocity pressure q, combining Equations B.12 and B.13 gives the probability that q be the extreme velocity pressure over a year:

$$F_q^1(q) = P(0,1) = \exp\left(-\exp\left(-\frac{q - \alpha_q}{\beta_q}\right)\right) \tag{B.17}$$

where α_q and β_q, called the location and scale parameters, can be related the standard deviations of X and $\dot{X}$. Such a distribution is called a Fisher-Tippett Type 1 distribution. It can be derived that:

$$\mu_q^1 = \alpha_q + \gamma\beta_q \qquad \sigma_q^1 = \frac{\pi}{\sqrt{6}}\beta_q \tag{B.18}$$

It is to be noted that the variable is different in Equations B.14 and B.17, and mean values determined subsequently. In B.14, the variable is the duration before an upcrossing. In B.17, the variable is the value of the threshold that will not be exceeded during one year. The extreme velocity pressure over T years also follows a Type 1 distribution, related to the distribution of annual extreme values by:

$$\mu_q^T = \mu_q^1 + \beta_q \ln(T) \qquad \sigma_q^T = \sigma_q^1 \tag{B.19}$$

The following relation is often used to derive the 50-years velocity pressure. It relates the velocity pressure q and the annual probability of exceedence of $p = 1 - F_q^1(q)$. For T=50 years, p=0.02:

$$\frac{q(p)}{q_{50}} = \frac{1 - K_q \ln(-\ln(1-p))}{1 - K_q \ln(-\ln(0.98))}$$

(B.20)

Typically, $K_q \approx 0.2$.

APPENDIX C: TREATMENT OF STOCHASTIC PROCESSES

C-1 Definitions

The most common transformation applied to a deterministic load to process it is to compute its Fourier transform, and to work in the frequency domain:

$$Y(\omega) = \int_{-\infty}^{\infty} y(t)e^{-i\omega t}dt \qquad (C.1)$$

There are several limitations to the use of that formulation for stochastic processes. First, the result would also be a stochastic process, limiting its interest. But more essential is the fact that $Y(\omega)$ almost never exists for a stationary process like those used in wind engineering. The condition of existence for the Fourier transform, a condition of absolute integrability, is:

$$\int_{-\infty}^{\infty} |y(t)|dt < \infty \qquad (C.2)$$

A stationary process is one whose statistical properties are independent of time. Obviously, such a process cannot satisfy condition B.2. This is why is introduced the spectral density, as the Fourier transform of the spectral density:

$$S_X(n) = 4\int_0^{\infty} \kappa_X(\tau)\cos(2\pi n\tau)d\tau \qquad (C.3)$$

$$\kappa_X(\tau) = E\{(X(t)-\mu_X)(X(t+\tau)-\mu_X)\} \qquad (C.4)$$

Several useful relations can be derived then:

$$\kappa_x(\tau) = \int_0^{\infty} S_X(n)\cos(2\pi n\tau)d\tau \qquad (C.5)$$

$$\sigma_X^2 = \kappa_X(0) = \int_0^{\infty} S_X(n)dn \qquad (C.6)$$

Similarly, the cross-spectral density and the cross-correlation are defined by:

$$\kappa_{XY}(\tau) = E\{(X(t)-\mu_X)(Y(t+\tau)-\mu_Y)\} \qquad (C.7)$$

$$S_{XY}(n) = 2\int_{-\infty}^{\infty} \kappa_{XY}(\tau)\exp(-i2\pi n\tau)d\tau \qquad (C.8)$$

Stationarity of the stochastic processes guarantees that κ_{XY} and S_{XY} are well-defined, i.e. independent of t. It is to be noted that S_X is real, while nothing guarantees this for S_{XY}.

61

C-2 Response of linear systems

Using the impulse response function G(t), it is possible to relate the frequency response function H(n), and the spectral densities of the input and the output. f(t) is the input and x(t) the output of a linear system.

$$x(t) = \int_{-\infty}^{t} G(t-\tau)f(\tau)d\tau = \int_{0}^{\infty} G(\tau)f(t-\tau)d\tau \qquad (C.9)$$

$$X(n) = H(n)F(n) \qquad (C.10)$$

The timeline is extended to negative t for the purpose of integration, simply by taking f and x equal to zero before t=0. It then follows easily by combining C.3, C.4, C.9 and C.10:

$$S_X(n) = |H(n)|^2 S_F(n) \qquad (C.11)$$

C-3 Spatial correlation

Another useful spectral density is defined for processes X(P,t) varying in space:

$$S_{XX}(P_1, P_2, n) = 2\int_{-\infty}^{\infty} E\{X(P_1, t)X(P_2, t+\tau)\}\exp(-i2\pi n\tau)d\tau \qquad (C.12)$$

The normalized co-spectrum is then defined as the real part of the normalized spectral density:

$$\psi_X = \text{Re}\left\{\frac{S_{XX}(P_1, P_2, n)}{\sqrt{S_X(P_1, n)S_X(P_2, n)}}\right\} \qquad (C.13)$$

A widely used approximation, introduced by Davenport in 1962, assumes the normalized spectral densities of the turbulence components are real, and then equal to the normalized co-spectrums. It is very useful when determining the standard deviation of a response parameter R(t):

$$R(t) = \int_0^l I(y)u(y, t)dt \qquad (C.14)$$

$$\kappa_R(\tau) = E\{R(t)R(t+\tau)\}$$

$$\kappa_R(\tau) = \int_0^l \int_0^l I(y_1)I(y_2)E\{u(y_1, t)u(y_2, t+\tau)\}dy_1 dy_2$$

$$S_R(n) = \int_0^l \int_0^l I(y_1)I(y_2)\sqrt{S_u(y_1,n)}\sqrt{S_u(y_2,n)}\psi_u(r,n)dy_1dy_2$$

$$S_R(n) = \int_0^l k(r)\psi_u(r,n)dr \qquad (C.15)$$

where $k(r)$ is the co-influence function introduced in Appendix D:

$$k(r) = \int_0^{l-r} I(y)\sqrt{S_u(y,n)}I(y+z)\sqrt{S_u(y+z,n)}dn \qquad (C.16)$$

Most often, reference values of I and S_u are introduced, to work with dimensionless functions, and to remove the dependence of $k(r)$ in the frequency n. The last relies on the assumption that $\dfrac{S_u(y,n)}{S_u(y_{ref},n)}$ is effectively independent of n. It follows:

$$S_R(n) = \left(I_{ref}\sqrt{S_u(y_{ref},n)}\right)^2 \int_0^l \int_0^{l-r} g(y)g(y+r)dy\psi_u(r,n)dr \qquad (C.17)$$

$$g(y) = \frac{I(y)}{I_{ref}}\sqrt{\frac{S_u(y,n)}{S_u(y_{ref},n)}} \qquad (C.18)$$

APPENDIX D: MULTIPLE INTEGRALS

The correlation function often leads to integrals of the form:

$$I = \int_0^1 \int_0^1 g(y_1)g(y_2)f(s)dy_1 dy_2 \qquad (D.1)$$

where $s = |y_1 - y_2|$. This integral can be simplified in the following way:

$$I = \int_0^1 \int_0^{y_1} g(y_1)g(y_2)f(s)dy_2 dy_1 + \int_0^1 \int_{y_1}^1 g(y_1)g(y_2)f(s)dy_2 dy_1$$

$$I = \int_0^1 \int_0^{y_1} g(y_1)g(y_1-s)f(s)dsdy_1 + \int_0^1 \int_0^{1-y_1} g(y_1)g(y_1+s)f(s)dsdy_1$$

$$I = \int_0^1 \int_s^1 g(y_1)g(y_1-s)f(s)dy_1 ds + \int_0^1 \int_0^{1-s} g(y_1)g(y_1+s)f(s)dy_1 ds$$

The last equality is classical in the theory of multiple integral. It has a simple geometrical meaning. The function in the integral is being integrated over a triangle. To compute I, it does not change the result to integrate "vertically" or "horizontally".
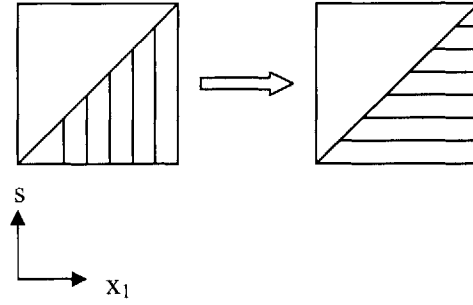

Figure D - 1: Multiple integral transformation

Analytically:

$$\int_0^1 \int_0^{x_1} dsdx_1 = \int_\Delta dS = \int_0^1 \int_s^1 dx_1 ds \qquad (D.2)$$

where $\Delta = \left\{ (s, x_1) \in (0,1)^2 \mid s \le x_1 \right\}$.

Finally, substituting x_1 for $x+s$, I can be written as a function of the co-influence function $k(s)$:

$$I = \int_0^1 k(s)f(s)ds \qquad (D.3)$$

$$k(s) = 2 \int_0^{1-s} g(s)g(x+s)dx \qquad (D.4)$$

A linear system is usually characterized by a series of modes and modal properties: mode shape ξ_i, circular frequency ω_i or frequency n_i, damping ratio ζ_i. The frequency response function of the system for the ith mode $H_i(n)$ then verifies:

$$|H_i(n)|^2 = \frac{1}{k^2} \frac{1}{(1-\Omega_i^2)^2 + 4\zeta_i^2\Omega_i^2}$$ (E.1)

where $k = m_i\omega_i^2$ and $\Omega = \dfrac{\omega}{\omega_i} = \dfrac{n}{n_i}$. It is beyond the scope of this text to expose in detail the theory of structural dynamics. However a useful simplification is possible in wind engineering, based on the very selective nature of $H_i(n)$ and the low frequencies involved in wind load. Figure 2-1 shows that most of the frequency content of wind, even turbulent wind, is above periods of 30 s. Conversely, it is rare (and undesirable, or the bridge would enter resonance too easily) that the fundamental frequency of a bridge be that high.
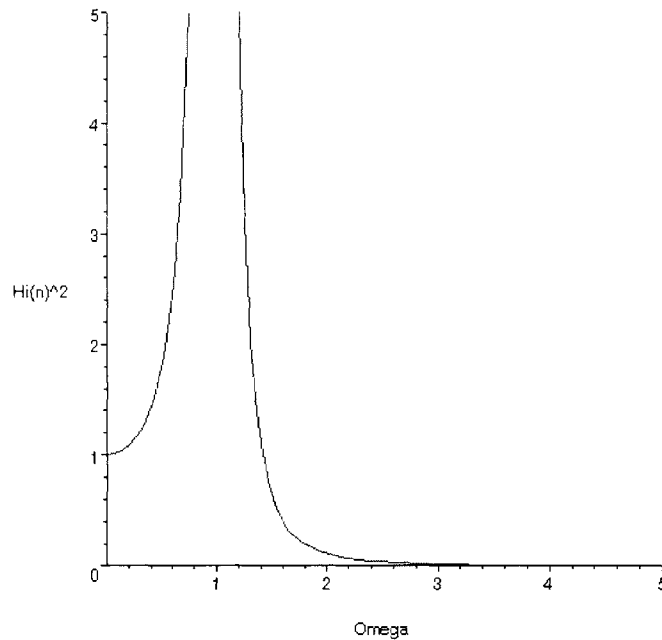

Figure E - 1: Plot of the frequency response function against Ω (ζ=0.02)

It is often necessary in wind engineering to compute integrals such as:

$$I = \int_0^\infty F(n) |H_i(n)|^2 \, dn \tag{E.2}$$

Assuming that damping is low ($\zeta_i \ll 1$) and $F(n)$ has most of its values at frequencies below n_i, I can be approximated by:

$$I = |H_i(0)|^2 \int_0^\infty F(n) dn + F(n_i) \int_0^\infty |H_i(n)|^2 \, dn \tag{E.3}$$

$\int_0^\infty |H_i(n)|^2 \, dn$ cannot be calculated in a classical way. It is necessary to use contour integration. The result, involving the logarithmic decrement $\delta_i \approx 2\pi\zeta_i$ (for small values of damping) gives:

$$\int_0^\infty |H_i(n)|^2 \, dn = \frac{1}{m_i^2} \frac{n_i}{(2\pi n_i)^4} \frac{\pi^2}{2\delta_i} = \frac{n_i}{k^2} \frac{\pi^2}{2\delta_i} \tag{E.4}$$